Controlling the Quantum

Creating a protocol for arbitrary state generation in an LC oscillator using Jaynes-Cummings interactions

Marijn Morssink

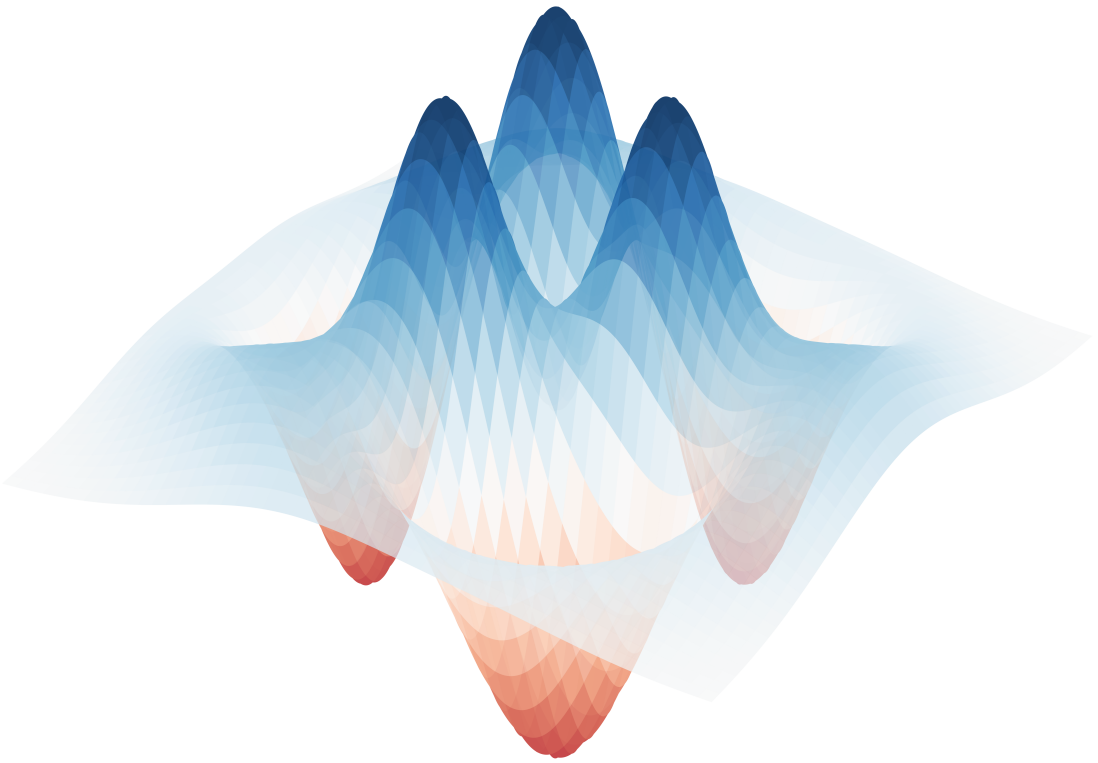

Controlling the Quantum

Creating a protocol for arbitrary state generation in an LC oscillator using Jaynes-Cummings interactions

by

Marijn Morssink

to obtain the degree of Bachelor of science
at the Delft University of Technology,
to be defended publicly on Wednesday June 26, 2024 at 10:00 AM.

Student number:	5642078	
Project duration:	March 14, 2024 – June 26, 2024	
Thesis committee:	Prof. dr. G. A. Steele,	supervisor TN
	Dr. S. K. J. Aerts,	supervisor TW
	Dr. P. M. Visser,	second committee member TW
	Dr. M. Rossi,	second committee member TN
	S. Deve,	PhD supervisor

TU Delft

Abstract

Producing arbitrary quantum states in mechanical oscillators is an essential part of the research concerning combining the theory of quantum mechanics with general relativity. In recent years, a lot of progress was made by the development of optomechanics and circuit quantum electro dynamics using which a quantum mechanical interaction between an LC oscillator and a mechanical oscillator can be created. This only left the need for the ability to create arbitrary desired states in an LC oscillator while keeping its properties as a linear resonator in tact. The interaction needed for this was recently designed in the group and is called the photon-pressure interaction. Using this interaction, effectively a Jaynes-Cummings interaction between a qubit and a LC oscillator was created which can truly be turned on and off, keeping the linear properties of the LC oscillator while the interaction is turned off. In this thesis a protocol that makes use of the Jaynes-Cummings interaction and qubit drives to create arbitrary states in the LC oscillator is developed. To show that the desired oscillator state has been created a protocol is also developed to perform Wigner tomography on the LC oscillator. Both protocols have been tested using simulations with loss effects corresponding to the ones encountered in our lab setting. The simulation results show that using the current lab system settings, states can successfully be produced in the LC oscillator and measured using the tomography protocol. This paves the way for arbitrary state generation and state measurement experimentally in the lab.

Acknowledgements

The past few months working on and finishing my thesis at Steelelab have been an amazing experience. Learning new physics, using it and being able to discuss with other people about it is something I was hoping to do one day when I first started my bachelor. The fact that my thesis project is ending feels a bit sudden as I was enjoying it a lot. Therefore, I want to thank a couple of people who helped me and made my thesis such a nice experience. First I want to thank Sven Aerts who was my mathematics supervisor, for giving the space to do a project I wanted and not being restricted to much by the mathematics side. I also want to thank Gary Steele who was my physics supervisor and provided the opportunity to be part of this group and do this project which was exactly the sort of project I was looking for. I want to thank Robin Dekker for showing me around the lab and showing the experimental en technical perspective on the matter.
Finally, I want to thank Sercan Deve, who has read and corrected my thesis countless times and guided me along during the project. We have had a lot of meetings together during which we have had interesting discussions, these were some of the things I enjoyed the most during my thesis.

Contents

Chapter 1

Introduction

The ability to create arbitrary quantum states is of great use for experimental as well as practical applications in quantum mechanics. One of the fields where this control is of use is in the research of combining the theory of quantum Mechanics with General Relativity. Both theories have stood alongside eachother for a century, however, attempts at combining the two have yet to be successful. To make progress in this research, devices that have the capability of measuring quantum effects as well as the effects of gravity have to be engineered. This is a difficult task as quantum mechanics is most prevalent at very small scales, while due to the weak nature of gravity quite large and heavy objects are needed to measure gravity effects. One needs a system that is small enough to measure the effects of quantum mechanics, but large enough to measure the effects of gravity. A more complete description of the problem and more exact bounds on the sytem parameters are given in [1]. The relatively new field of (cavity) optomechanics has braught new mechanisms to the table for creating such a device [2]. Optomechanics studies the interactions of light with mechanical moving systems at the micro scale. This interaction makes it possible to create quantum mechanical superpositions states in mechanical oscillators that can be around $200\mu m$, one such oscillator is shown in figure 1.1 (b). The specifics and deeper theory of optomechanics are outside the scope of this thesis, an overview of the basics of optomechanics may found in [3].

One can first create a desired state in for example a LC oscillator and then using an optomechanical interaction transfer this state to the mechanical oscillator[4][5]. Due to the fact both resonators are linear and in the correct regime the interaction is linear, this is a relatively simple procedure. The only thing that still has to be done is creating the desired state in the LC-oscillator. The full process of creating a state in the mechanical oscillator is shown in figure 1.1 (a) and an example of an LC oscillator is shown in 1.1 (c).

Creating quantum mechanical states in the oscillator is however not trivial, since this can not be done using classical drives and interactions. To create an arbitrary quantum state a non-linear element is needed[6]. This element will be a superconducting qubit, which is highly non-linear as it only has two effective states. Superconducting qubits are circuits which make use of the effects of superconductivity and quantum mechanics to create a non-linear element[7][8][9]. The qubit is needed since it can be brought into an arbitrary quantum state by applying classical drives to it [8]. Then using a suitable quantum mechanical interaction between the Qubit and the oscillator, the oscillator may also be brought into a quantum mechanical state. A suitable interaction for this is the Jaynes-Cummings interaction. In [6] it has been shown that using this interaction, arbitrary states may be produced in a LC oscillator. In general however, the Jaynes-Cummings interaction is brought into the system using a capacitive coupling between the qubit and oscillator. This interaction can be set to be very weak after having generated the desired oscillator state by increasing the detuning between the oscillator and qubit, by using a tunable qubit. However, it can never be set truly of. Large detuning gives rise to the “dispersive interaction"’[10] which will lead to entanglement between the oscillator and the qubit [11]. This leads to problems in the further procedure of swapping the state from the LC-oscillator to the mechanical oscillator, as now the LC-oscillator is not linear any more due to the coupling with the qubit. The non-linearity of the LC-oscillator means that the swap using the previously mentioned

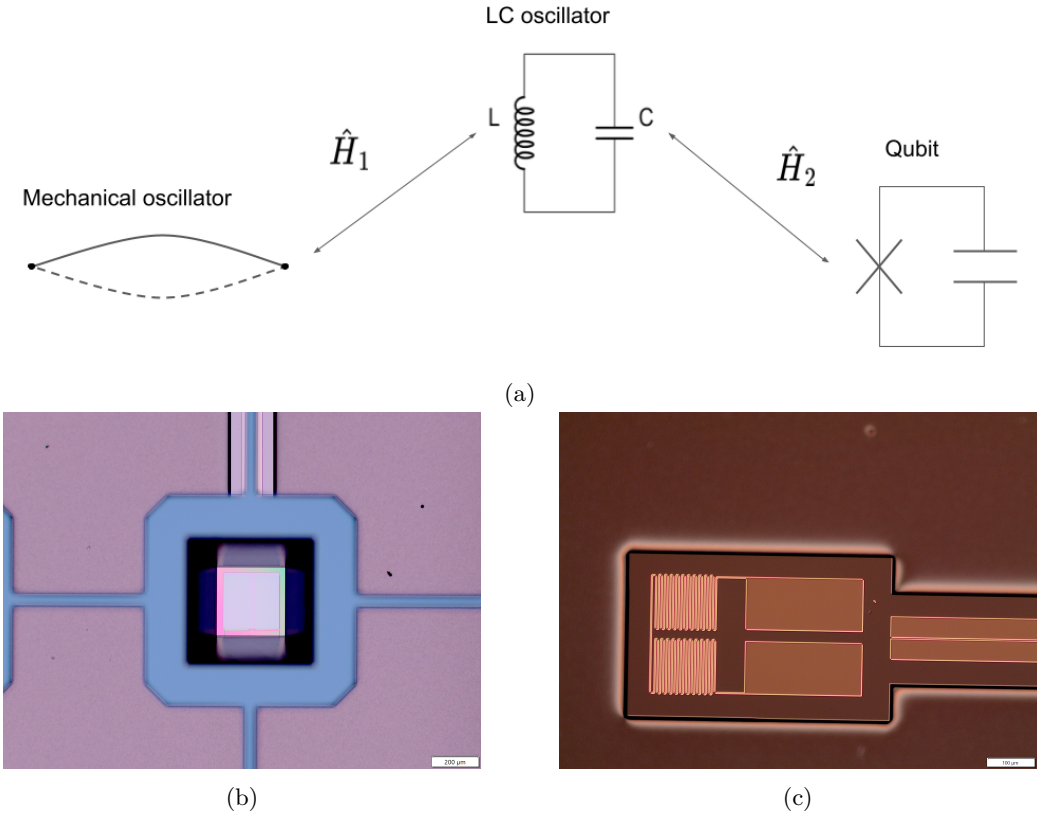

(a)

(b)

(c)

Figure 1.1: (a) shows a schematic of the system for creating arbitrary quantum states in a mechanical oscillator. The indicated components interact via interactions with Hamiltonians indicated by $\hat{H}_1$ and $\hat{H}_2$. Figure (b) shows an image of the membrane chip which forms the mechanical oscillator. The light square is the membrane of the oscillator. The scale indicator at the bottom right of the image is $200\mu m$. Figure (c) shows an image of a LC oscillator, the scale indicator at the botom right of the image is $100\mu m$. The capacitance of the LC oscillator is formed by its own capcitor plates and the mebrane from (b) which is right above it. The two big light rectangles in (c) are capacitor plates of one side of the capacitance, the membrane shown in (b) forms the other capacitor plate of the capacitance. The two long "beams" in the right of (c) are the transmission lines going to the LC circuit used to send signals to end receive signals from the oscillator.

linear optomechanical coupling can not be performed properly anymore. To solve this issue, a new method of coupling the qubit to the LC-oscillator was designed in our group[12], which was named photon-pressure coupling. Under the application of the correct drive this photon-pressure coupling will act as a Jaynes-Cummings type of interaction[12], with the added benefit that it can be turned truly on or off. By turning off the coupling the LC-oscillator is effectively linear again, which means the linear interaction between the LC-oscillator and mechanical oscillator can be used effectively. An added benefit of this new interaction is that the phase of the interaction can be dynamically controlled, which is not possible with the standard capacitive Jaynes-Cummings interaction.
A theoretical procedure for generating arbitrary states using the Jaynes-Cummings interaction has been proposed in [13]. This method has partially been performed in practice as shown in [6] using superconducting circuits. However, instead of using two types of operations as proposed in [13], three were used. This was because with the capacitively induced Jaynes-Cummings interaction it is not possible to control the phase of the interacion. [14] synthesizes Fock states and superposition states of $|0\rangle$ and $|1\rangle$ in an acoustic wave-resonator. However for the production of these states a complex algorithm is not needed. In [15] the procedure explained in [13] is used on a Be^+ ion confined by a harmonic potential instead of a superconducting circuit.

Measuring the produced state in the oscillator is an important final step to validate if the prescribed

procedures are actually able to create the desired state in the LC oscillator. The procedure of measuring the full state of the oscillator is called Wigner tomography, which aims to reconstruct the Wigner function of a quantum state. One method of tomography “reuses" the Jaynes-Cummings interaction to perform readout of the oscillator state using a qubit. This method has been performed experimentally in [14] and [6].

This thesis will use the methods proposed by [13] to create a program which can give the needed parameters for the protocol to create any desired arbitrary state in the LC oscillator. A program to simulate the state construction procedure will also be created such that the designed algorithm can be tested.

Using the simulation the effects of decay and dephasing on the results of the construction procedure will be investigated. The simulations will also be used to find construction limits considering the imperfections of the real world setup. As an extra part, this thesis will also cover the tomography method used in [14] and [6] to measure the Wigner function of oscillator states. The tomography will also be simulated using lab system values to investigate how the best Wigner functions may be measured in the lab system.

Chapter 2

Theory

In this chapter, an overview of the needed physics will be given. In the first sections, we will look at the Jaynes-Cummings model. We will look at how it is derived and some of its useful properties. In the second section we will take a look at some parts of circuit quantum dynamics, such that we can couple the knowledge of the Jaynes-Cummings model to our physical setups in the lab. In the third section we will look at how we can construct an algorithm using the pre-gained theoretical knowledge.

Throughout the theory chapter and the rest of the paper, we will use units where $\hbar = 1$ for brevity.

2.1 The Jaynes-Cummings model

The Jaynes-Cummings model is originally a model that was developed to describe the interaction between an atom and a single mode light cavity in quantum optics[10]. However, the model and the form of the Hamiltonian are not restricted to just atom light interactions and can for example also be used in circuit quantum electrodynamics, as will be done in this paper. The thing that makes the Jaynes-Cummings model special, is that it quantizes the electro-magnetic field in the cavity, instead of using a classical representation.

In the first part of this section, the model will be derived from the atom-field perspective. Other important features of the model will also be derived. In the second part of this section, it will briefly be shown how this model may also be applied to quantum circuits.

2.1.1 Atom light interaction

The Jaynes-Cummings model describes the interaction between a two state atom and a single mode light cavity. For the atom, we will consider an electron bound to an atom. Since both the light field and the atom are quantized, there will be creation and anihilation operators for both. The creation and anihilation operators for the field will be denoted $\hat{a}^\dagger$ and $\hat{a}$. For the two state atom, we will define: $|e\rangle\langle g|\hat{\sigma}^\dagger$ and $|g\rangle\langle e| = \hat{\sigma}$, where $|g\rangle$ and $|e\rangle$ denote the ground and excited state of the atom respectively. The separate Hamiltonians of the field with frequency ω and atom with freqency ω_0 may then be written as:

$$\begin{aligned} \hat{H}_{field} &= \omega \hat{a}^\dagger \hat{a} \\ \hat{H}_{atom} &= -\frac{\omega_0}{2}\hat{\sigma}_z, \end{aligned} \tag{2.1}$$

where we omitted the factor $\frac{1}{2}$ corresponding to the zero point energy from the cavity field Hamiltonian, σ_z is the pauli spin matrix in z direction and we added a minus sign in the atom Hamiltonian as a convention.

Starting from a classical perspective, we can also derive the interaction Hamiltonian of the field and the atom. We can approximate the interaction between the light field and the atom to only consist of

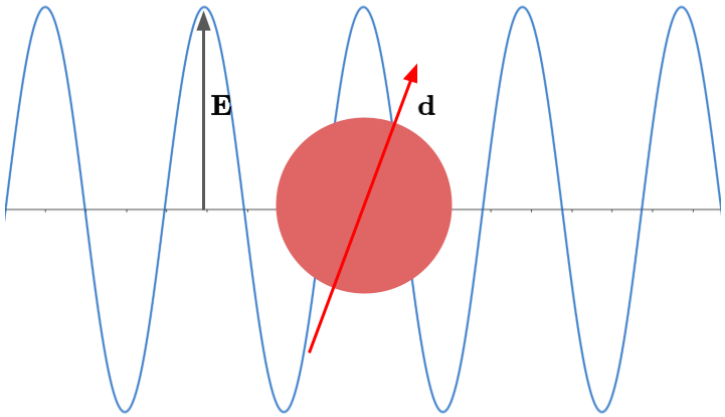

Figure 2.1: schematic of atom in a single mode field. The field vector is indicated by **E** and the atom dipole moment by **d**

the interaction between the dipole moment of the atom and the electric field of the light field[10]. This would yield the following term for the energy of the interaction:

$$E = -\mathbf{d} \cdot \mathbf{E}, \tag{2.2}$$

where **d** represents the dipole moment of the atom and **E** represents the electric field. In the case of our atom with one electron, this dipole moment would be given by $-e\mathbf{r}$ where **r** is just the relative position of the electron with respect to the nucleus.

Now, switching to a quantum mechanical perspective, we (naively) swap the classical dipole moment and field for their respective quantum mechanical operators:

$$\hat{H}_{int} = -\hat{\mathbf{d}} \cdot \hat{\mathbf{E}}. \tag{2.3}$$

The electric field operator may be written as $\hat{\mathbf{E}} = \varepsilon \mathbf{e}(\hat{a} + \hat{a}^\dagger)$, as shown in [10]. Here **e** is the unit vector which gives the direction of the polarization of the field. Then as shown in [10] we can write $\hat{\mathbf{d}} \cdot \mathbf{e} = d\hat{\sigma} + d^*\hat{\sigma}^\dagger$. Using this we find for the complete interaction Hamiltonian:

$$\begin{aligned} \hat{H}_{int} &= \varepsilon(\hat{a} + \hat{a}^\dagger)(d\hat{\sigma} + d^*\hat{\sigma}^\dagger) \\ &= (\hat{a} + \hat{a}^\dagger)(g^*\hat{\sigma} + g\hat{\sigma}^\dagger). \end{aligned} \tag{2.4}$$

Normally, in literature, d is considered real, however, further on in this paper we will use cases where the coupling $g = \varepsilon d^*$ does in fact have a phase.

Putting the free Hamiltonians and the interaction Hamiltonians together, we find the following full Hamiltonian describing our system:

$$\hat{H} = \omega\hat{a}^\dagger\hat{a} - \frac{\omega_0}{2}\hat{\sigma}_z + (\hat{a} + \hat{a}^\dagger)(g^*\hat{\sigma} + g\hat{\sigma}^\dagger). \tag{2.5}$$

There is one more approximation that is often considered when using this hamiltontian, and we will use it as well. Writing the Hamiltonian in the interaction picture [16], using $\hat{H}_0 = \omega\hat{a}^\dagger\hat{a} - \frac{\omega_0}{2}\hat{\sigma}_z$, we find:

$$\hat{H}_{int}(t) = g^*\hat{a}\hat{\sigma}e^{-i(\omega+\omega_0)t} + g\hat{a}^\dagger\hat{\sigma}^\dagger e^{i(\omega+\omega_0)t} + g\hat{a}\hat{\sigma}^\dagger e^{i(-\omega+\omega_0)t} + g^*\hat{a}^\dagger\hat{\sigma}e^{i(\omega-\omega_0)t}. \tag{2.6}$$

We will now apply the so called rotating wave approximation and drop the high frequency terms, since these will "average out" over time compared to the low frequency terms when ω_0 is sufficiently close to ω. Intuitively, this approximation could also be seen as dropping the "non energy conserving" terms, since the terms that are dropped correspond to excitation or de-excitation of both the field and the atom at the same time. Dropping these terms leaves us with the final Jaynes-Cummings Hamiltonian that we will use further:

$$\hat{H}_{JC} = \omega \hat{a}^\dagger \hat{a} - \frac{\omega_0}{2}\hat{\sigma}_z + g^* \hat{a}^\dagger \hat{\sigma} + g \hat{a} \hat{\sigma}^\dagger \tag{2.7}$$

.

2.1.2 Properties of the Jaynes-Cummings model

The Jaynes-Cummings model has some interesting and useful properties. These can derived and understood the easiest by introducing the so-called Jaynes-Cummings ladder, which is nothing more than the set of eigenstates, $|n\rangle \otimes |e\rangle = |n, e\rangle$ and $|n\rangle \otimes |g\rangle = |n, g\rangle$ for $n \geq 0$, of the Jaynes-Cummings hamiltontian without the interaction terms. Doing some general calculations shows which of these ladder states will interact:

$$\begin{aligned} \hat{a}\hat{\sigma}^\dagger |n, g\rangle &= \sqrt{n}|n-1, e\rangle \\ \hat{a}^\dagger \hat{\sigma} |n-1, e\rangle &= \sqrt{n}|n, g\rangle \\ \hat{a}\hat{\sigma}^\dagger |n-1, e\rangle &= 0 \\ \hat{a}^\dagger \hat{\sigma} |n, g\rangle &= 0 \end{aligned} \tag{2.8}$$

We see that the only off diagonal, interaction terms, of the Hamiltonian will be between states of the form $|n, g\rangle$ and $|n-1, e\rangle$. Since the interactions come in pairs, it is easiest to investigate the individual 2D subspaces of interacting pairs. The interacting pairs are formed by the states $|n-1, e\rangle$ and $|n, g\rangle$, which span a 2D subspace (for $n \geq 1$). If we use the convention:

$$\alpha |n-1, e\rangle + \beta |n, g\rangle = \begin{pmatrix} \alpha \\ \beta \end{pmatrix}, \tag{2.9}$$

we can write the Hamiltonian of the subspace in the following form:

$$\hat{H}_n = \begin{pmatrix} \omega(n - \frac{1}{2}) - \frac{\Delta}{2} & g\sqrt{n} \\ g^*\sqrt{n} & \omega(n - \frac{1}{2}) + \frac{\Delta}{2} \end{pmatrix}, \tag{2.10}$$

where $\Delta = \omega - \omega_0$ is the detuning of the field and qubit frequencies and the $\sqrt{n}$ follows from the creation and annihilation operators of the oscillator. Solving for the eigenenergies and states yields:

$$E_{n\pm} = \pm\sqrt{|g|^2 n + \frac{\Delta^2}{4}} + \omega(n - \frac{1}{2}) \tag{2.11}$$

and

$$\begin{aligned} |\psi_{n+}\rangle &= e^{i\theta}\frac{\sqrt{\Omega_n - \Delta}}{\sqrt{2\Omega_n}}|n-1, e\rangle + \frac{\sqrt{\Omega_n + \Delta}}{\sqrt{2\Omega_n}}|n, g\rangle \\ |\psi_{n-}\rangle &= -e^{i\theta}\frac{\sqrt{\Omega_n + \Delta}}{\sqrt{2\Omega_n}}|n-1, e\rangle + \frac{\sqrt{\Omega_n - \Delta}}{\sqrt{2\Omega_n}}|n, g\rangle \\ \Omega_n &= 2\sqrt{|g|^2 n + \Delta^2} \end{aligned} \tag{2.12}$$

In the resonant case ($\Delta = 0$) the interaction leads to splitting of the degenerate eigenenergies and in the non-resonant case, it leads to larger differences in the eigen energies of the interacting pairs, also

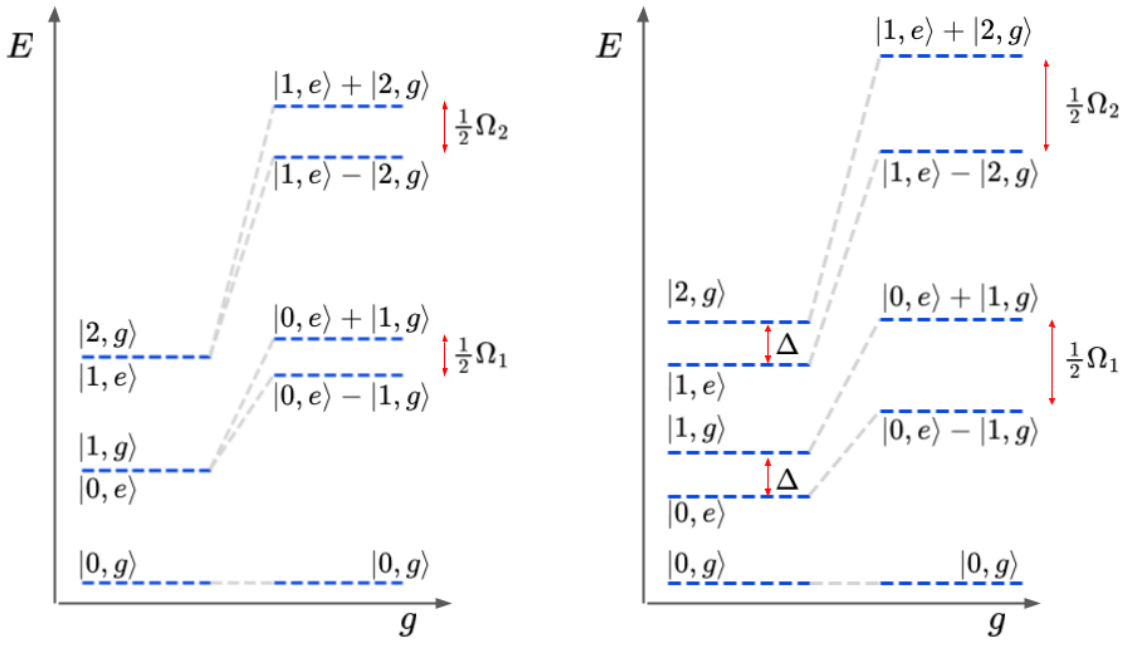

(a) (b)

Figure 2.2: In (a) a schematic of the first five energy levels of the Jaynes-Cummings model with $\Delta = 0$. The diagram shows the splitting of the degenerate energy levels for increasing g. The energy levels are indicated with their corresponding eigenstates. The resulting gaps are indicated by the red arrow. Ω_n is the size of the gaps and is defined as $\Omega_n = \sqrt{|g|^2 n + \frac{\Delta^2}{4}}$. In (b) a similar schematic but with $\Delta \neq 0$. Here there is also splitting due to the detuning, indicated by the red arrows with the Δ. Ω_n is again defined as in (a)

shown in figure 2.5b. These new eigenstates are often called dressed states.

Due to the form of the eigenstates, it seems that the interaction will lead to some kind of oscillations between the states $|n-1, e\rangle$ and $|n, g\rangle$.

Later, in section 2.1.3, we will derive the full time-evolution operator of the system, for now we will take a look at a simpler case and solve the system for the initial state $|0, e\rangle$ in the resonant case ($\Delta = 0$). Using $|0, e\rangle = \frac{1}{\sqrt{2}}(|\psi_{1+}\rangle - |\psi_{1-}\rangle)$ We can write the general state as

$$|\psi\rangle(t) = \frac{1}{2}(e^{-iE_{1+}t}|\psi_{1+}\rangle - e^{-iE_{1-}t}|\psi_{1-}\rangle) \tag{2.13}$$

Substituting 2.11 and writing $|\psi\rangle(t)$ in terms of $|0, e\rangle$ and $|1, g\rangle$ yields

$$|\psi\rangle(t) = e^{-i\frac{1}{2}\omega t}(\cos(|g|t)|0, e\rangle - i\frac{g}{|g|}\sin(|g|t)|1, g\rangle) \tag{2.14}$$

Using this, we can also find $P_e(t)$, the excited state probability of the atom.

$$P_e(t) = \frac{1}{2} + \frac{1}{2}\cos(2|g|t) \tag{2.15}$$

We indeed find so called Rabi-oscillations between the interacting states. With in this case the Rabi frequency $\Omega_1 = 2|g|$. See figure 2.3.

In general the Rabi frequency for a pair of interacting states is given by $\Omega_n = 2|g|\sqrt{n}$.

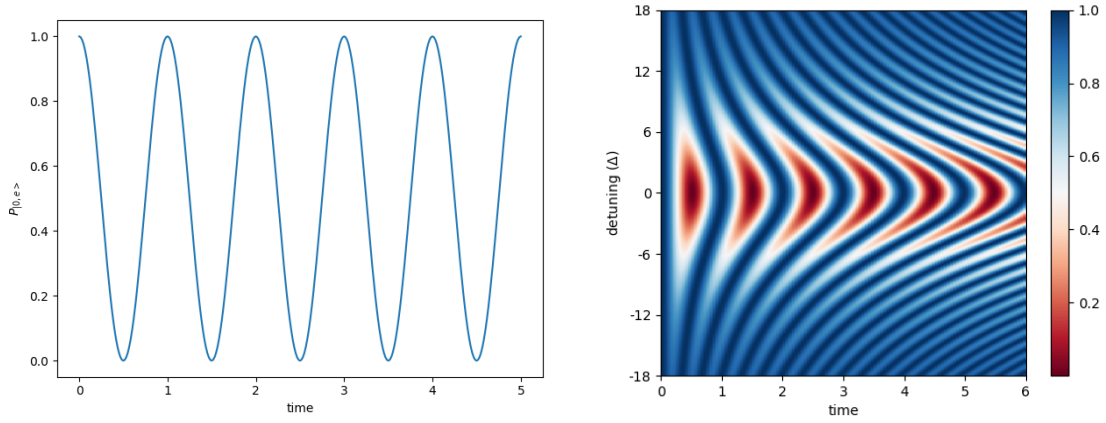

(a) (b)

Figure 2.3: In (a) a numerical solution of the excited state probability of the $|0, e\rangle$ state over time. The trace matches the analytically derived solution 2.15. The parameters where chosen $\omega = \omega_0 = 2\pi$ and $g = \pi$, such that one oscillation matches one unit of time. In (b) a plot showing the effect of detuning Δ on the $|0, g\rangle$ probability. Values are again numerical solutions. The colors indicate the probability with values as indicated in the color bar. Parameters apart from detuning are the same as in (a). Detuning Δ is in the same units as ω and ω_0.

One important consequence of these frequencies being proportional to $\sqrt{n}$ is that if you start with a superpositon of the form $|\psi\rangle = (\sum a_n|n\rangle) \otimes |g\rangle$, where the field and the atom are disentangled, applying the Jaynes-Cummings interaction will (nearly) always result in an entangled state of the form $|\psi\rangle = (\sum a_n|n\rangle|g\rangle + b_n|n\rangle|e\rangle$.

The effects of detuning on the evolution of the system can be found using the same method as above with $\Delta \neq 0$. However, the most important features can be learned easier from an image from a simulation. Consider again an initial state $|0, e\rangle$. Simulating this initial state using equation 2.7 for different values of Δ and plotting $P_e(t)$, the excited state probability of the atom, leads to figure 2.3 (b), which neatly summarizes the effects of the detuning. The larger the detuning, the less the amplitude of the Rabi oscillations and the higher the oscillation frequency, most of the state population does not leave the initial state in this case. This can be seen by the fact that for large detuning the colors of the graph stay blue, which means they are close to 1. The lower oscillation amplitude is important, since this means that swaps between interacting states will not swap the full population of the states, but only part of it.

2.1.3 Derivation of time evolution operator

The time evolution operator of the Jaynes-Cummings model in the rotating wave approximation form, 2.7, can be calculated analytically. This is done easiest by looking at the form of the hamiltonitan, by realizing that the interactions of 2.7 between states only come in pairs. Hence we only need to look at the individual subspaces of interacting states and derive their time evolutions and can later easily combine them to get the full time evolution operator. The interacting pairs are formed by the states $|n-1, e\rangle$ and $|n, g\rangle$, which span a 2D subspace (for $n \geq 1$). If we use the convention:

$$\alpha|n-1, e\rangle + \beta|n, g\rangle = \begin{pmatrix} \alpha \\ \beta \end{pmatrix}. \tag{2.16}$$

We can write the Hamiltonian of the subspace in the following form:

$$\hat{H}_n = \begin{pmatrix} \omega(n - \frac{1}{2}) - \frac{\Delta}{2} & g\sqrt{n} \\ g^*\sqrt{n} & \omega(n - \frac{1}{2}) + \frac{\Delta}{2} \end{pmatrix}, \tag{2.17}$$

where $\Delta = \omega - \omega_0$ is the detuning of the field and qubit frequencies and the $\sqrt{n}$ follows from the creation and annihilation operators of the oscillator. Solving for the eigenstates yields:

$$E_{n\pm} = \pm\sqrt{|g|^2 n + \frac{\Delta^2}{4}} + \omega(n - \frac{1}{2}). \tag{2.18}$$

In the resonant case, $\Delta = 0$, we have $E_\pm = \pm|g|\sqrt{n} + \omega(n - \frac{1}{2})$. This yields the following eigenstates:

$$\begin{aligned} |\psi_{n+}\rangle &= \frac{1}{\sqrt{2}}\begin{pmatrix} e^{i\theta} \\ 1 \end{pmatrix} = \frac{1}{\sqrt{2}}(e^{i\theta}|n-1, e\rangle + |n, g\rangle) \\ |\psi_{n-}\rangle &= \frac{1}{\sqrt{2}}\begin{pmatrix} -e^{i\theta} \\ 1 \end{pmatrix} = -\frac{1}{\sqrt{2}}(e^{i\theta}|n-1, e\rangle + |n, g\rangle), \end{aligned} \tag{2.19}$$

where we wrote $g = |g|e^{i\theta}$. Since these are eigenstates of a time independent Hamiltonian, their time propagation is given by $|\psi_{n\pm}\rangle(t) = U_n(t)|\psi_{n\pm}\rangle = e^{-i\hat{H}_n t}|\psi_{n\pm}\rangle = e^{-iE_\pm t}|\psi_{n\pm}\rangle$ Then, using these states and given an initial state $|\psi_{init}\rangle = \alpha|n-1, e\rangle + \beta|n, g\rangle$

$$\begin{aligned} |\psi\rangle(t) &= e^{-i\hat{H}_n t}|\psi_{init}\rangle \\ &= e^{-i\hat{H}_n t}(\alpha * \frac{1}{\sqrt{2}}e^{-i\theta}(|\psi_+\rangle - |\psi_-\rangle) + \beta * \frac{1}{\sqrt{2}}(|\psi_+\rangle + |\psi_-\rangle)) \\ &= e^{-i\omega(n-\frac{1}{2})t}(\alpha \begin{pmatrix} \cos(|g|\sqrt{n}t) \\ -ie^{-i\theta}\sin(|g|\sqrt{n}t) \end{pmatrix} + \beta \begin{pmatrix} -ie^{i\theta}\sin(|g|\sqrt{n}t) \\ \cos(|g|\sqrt{n}t) \end{pmatrix}) \\ &= U_n(t)\begin{pmatrix} \alpha \\ \beta \end{pmatrix} \end{aligned} \tag{2.20}$$

From this we can now read of the time evolution matrix of the subspace:

$$\hat{U}_n(t) = e^{-i\omega(n-\frac{1}{2})t}\begin{pmatrix} \cos(|g|\sqrt{n}t) & -ie^{i\theta}\sin(|g|\sqrt{n}t) \\ -ie^{-i\theta}\sin(|g|\sqrt{n}t) & \cos(|g|\sqrt{n}t) \end{pmatrix}. \tag{2.21}$$

The full time evolution matrix is then given by:

$$\hat{U}_{JC}(t) = \begin{pmatrix} e^{i\frac{1}{2}\omega t} & & \ddots & & \\ & U_1(t) & & 0 & \\ \ddots & & \ddots & & \ddots \\ & 0 & & U_n(t) & \\ & & \ddots & & \ddots \end{pmatrix}. \tag{2.22}$$

2.2 Quantum Circuits

Circuit quantum electrodynamics is a rapidly growing field in the realm of quantum mechanics. The use of quantum circuits makes it possible to engineer desired systems and Hamiltonians for experiments and practical applications, for example creating artificial atoms and superconducting quantum computing. In the case of this paper, we will consider a circuit that is engineered to have the Jaynes-Cummings Hamiltonian 2.7. In this section, a brief overview of how to create the desired circuit will be given, as well as some further properties of the circuit that will be of use for this paper.

2.2.1 From quantum optics to circuits

The create the Hamiltonian of the form 2.7 using a circuit, the right components need to be chosen. The single-mode field cavity from the Jaynes-Cummings model will be replaced by a LC-oscillator. The two state atom will be represented by a qubit. Using these components, the desired interaction can be engineered.

2.2.1.1 Quantized LC-oscillator

The single-mode field will be replaced by a LC oscillator, which in this case is just a linear inductor coupled in parallel with a capacitor. The classical Hamiltonian of such a system, as derived in [8] is given by:

$$H = \frac{Q^2}{2C} + \frac{\Phi^2}{2L}. \tag{2.23}$$

Here Φ is the flux through the inductor and Q is the charge on the capacitor. Φ and Q are so-called conjugate variables where $\Phi = L\dot{Q}$ and $Q = C\dot{\Phi}$[8]. We can now quantize the circuit:

$$\hat{H} = \frac{\hat{\Phi}^2}{2L} + \frac{\hat{Q}^2}{2C}. \tag{2.24}$$

Because of the relation between Q and Φ, we can see that this Hamiltonian has a similar form as that of a harmonic oscillator,

$$\hat{H} = \frac{\hat{p}^2}{2m} + \frac{k\hat{x}^2}{2}, \tag{2.25}$$

where the $\hat{x}$ operator is replaced by $\hat{\Phi}$, the $\hat{p}$ operator is replaced by $\hat{Q}$ and the mass m and spring constant k are replaced by C and $\frac{1}{L}$ respectively. Using these similarities, can define an anihilation operator, similar to the harmonic oscillator, such that

$$\hat{H} = \omega(\hat{a}^\dagger\hat{a} + \frac{1}{2}) \tag{2.26}$$

with $\omega = \frac{1}{\sqrt{LC}}$ and

$$\begin{aligned} \hat{\Phi} &= \sqrt{\frac{L\omega}{2}}(\hat{a} + \hat{a}^\dagger) \\ \hat{Q} &= i\sqrt{\frac{C\omega}{2}}(\hat{a} - \hat{a}^\dagger). \end{aligned} \tag{2.27}$$

Since the LC oscillator represents a harmonic oscillator, we also get a similar eigenenergy and state structure, given by:

$$E_n = \omega(n + \frac{1}{2}) \tag{2.28}$$

With so called fock states, $|n\rangle$, as its eigenstates. A schematic of the energy levels is shown in 2.4 (a).

2.2.1.2 Qubits

To create an artificial two state atom, some device is needed that when in use effectively only has two states. A type of device with which this result can be obtained is the superconducting qubit. Superconducting qubits are devices that operate at very low temperatures (in the mK range). There are two main reasons such low temperatures are needed. The first one is that these temperatures are needed to obtain superconductivity in the circuits. For most frequently used materials, the critical temperures for superconductivity are in the range of a couple of Kelvins to in the tens of Kelvins [17]. However, this does not explain the need for temperatures in the mK. The need for the mK temperatures comes from the fact that the gap between the energy levels of the qubit is in the order of Ghz, and that the temperature fluctuations, k_bT are also in this range, when the temperatures are in the Kelvin range (temperature of photons of $1K$ have a frequency $\sim 20GHz$). This means temperature photons will be able to spontaneously excite the qubit to higher energy states which is undesired.

The most basic form of a qubit makes use of a so called Josephson-junction, which is acts as a non-linear inductor. The two important physical relations of the Josephson junction are:

$$\begin{aligned} I &= I_0 \sin(\phi), \\ V &= \frac{1}{2e}\frac{d\phi}{dt}. \end{aligned} \tag{2.29}$$

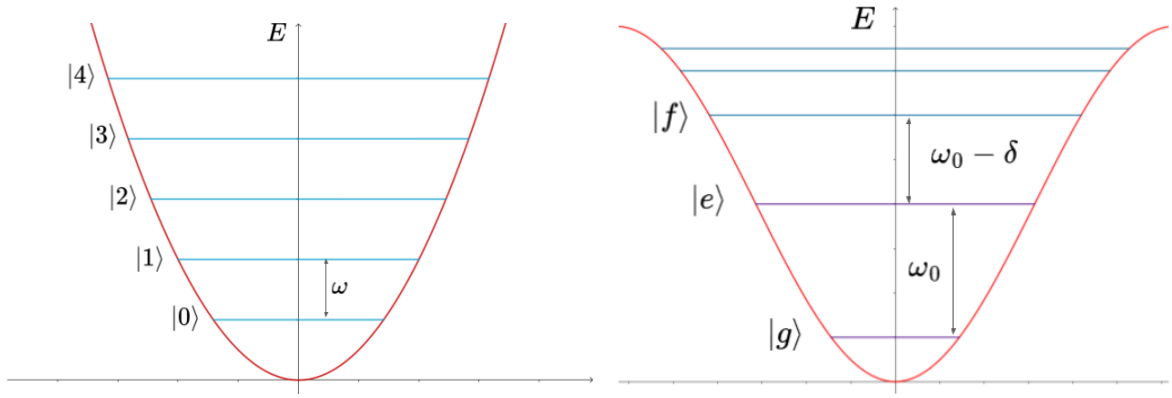

(a) (b)

Figure 2.4: Figure (a) shows the first five energy levels of the harmonics potential. The enrgy levels are indicated using their corresponding eigenstates. The spacing between the energy levels is equal for all energy levels and denoted by ω. Figure (b) shows a schematic of the energy levels of an anhamonic oscillator. In this case one with a sinusoidal potential such as the Josephson junction potential. The spacing between the first two levels, $|g\rangle$ and $|e\rangle$ is denoted by ω_0. To show the harmonicity, the third level $|f\rangle$ is also shown, where the difference in level spacing is denoted by δ. ω_0 is the effective frequency of the qubit.

To create a qubit, one can replace the linear inductor of the harmonic oscillator circuit by a Josephson junction. Since the Josephson junction also has a (typically very small) capacitance, the total capacitance of the qubit will be given by $C_q = C_J + C_s$ with C_s the capacitance of the customized oscillator. The s stands for shunt as this extra capacitor is often called a shunt capacitance. Replacing the inductor for the Josephson junction and writing $V_q = \frac{Q}{C_q}$ gives rise to the following Hamiltonian:

$$\hat{H} = \frac{\hat{Q}^2}{2C_q} - E_J \cos\left(\hat{\phi}\right), \tag{2.30}$$

where ϕ is the quantum phase difference between the two parts of the junction.

Writing $\hat{\Phi} = \hat{\phi}\Phi_0$, with $\Phi_0 = \frac{h}{2e}$, we find:

$$\hat{H} = \frac{\hat{Q}^2}{2C_q} - E_J \cos\left(\frac{\hat{\Phi}}{\Phi_0}\right). \tag{2.31}$$

The shunt capacitor is chosen such that $E_J \gg \frac{1}{C_q}$. This leads to the flux energy term dominating the Hamiltonian. This type of configuration is called a transmon qubit. The reason C_q is chosen such that $E_J \gg \frac{1}{C_q}$ is that when $E_J \ll \frac{1}{C_q}$, the charge term would be dominating, which would lead to a high sensitivity for charge noise [8]. Flux noise turned out to be easier to suppress, and thus the flux term was engineered to be dominating in the Hamiltonian [8].

We can view this Hamiltonian as instead of having a particle in a harmonic potential, having a particle in a cosinusoidal potential. When looking at one of the minima, the potential looks approximatly harmonic but not fully. Hence we can view this as a anharmonic oscillator. In this anharmonic oscillator, the energy levels all have different spacings, shown in figure 2.4b. Because of this, when operating at frequencies close to the frequency of the first energy gap, only interactions between the $|g\rangle$ and $|e\rangle$ state will happen and not between these and higher states. Therefore, when operating in the right frequency range, the anharmonic oscillator will function as a two state quantum system. We can now write the effective Hamiltonian of the qubit as:

$$\hat{H}_{qubit} = -\frac{\omega_0}{2}\hat{\sigma}_z, \tag{2.32}$$

where ω_0 is the frequency gap between the $|e\rangle$ and $|g\rangle$ states.

We can also define again the lowering and raising operators as $\hat{\sigma} = |g\rangle\langle e|$ and $\hat{\sigma}^\dagger$. And similarly to the harmonic oscillator, we can write:

$$\hat{Q} \propto i(\hat{\sigma} - \hat{\sigma}^\dagger). \tag{2.33}$$

There is a large variety of qubits which use these Josephson-junctions and some other components in different kinds of configurations, all with their own benefits and weaknesses, but the basic working principle is always based on the anharmonicity provided by the Josephson-junctions.

2.2.1.3 Qubit-Oscillator Jaynes-Cummings interaction

Having derived the quantized Hamiltonians for the qubit and LC-oscillator, only an interaction term between the two is needed to create a quantum circuit version of the Jaynes-Cummings Hamiltonian.

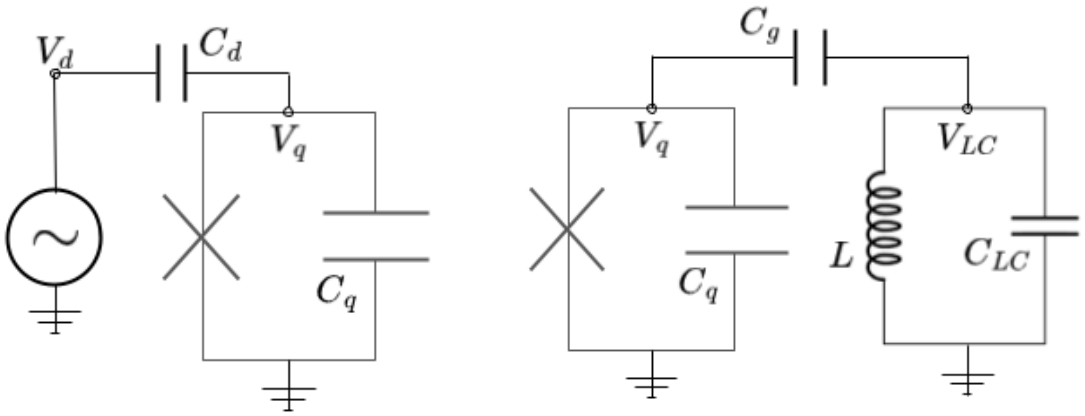

(a) (b)

Figure 2.5: Circuits with qubit. In (a) a circuit for driving a qubit. The voltage of the drive is defined as V_d and the voltage of the qubit as V_q. The capatcitance of the qubit is denoted C_q. The coupling capacitance to the drive is defined as C_q. (b) shows a circuit of a qubit coupled via a capacitance C_g to a LC oscillator. The qubit voltage is again defined V_q and the oscillator voltage is defined V_{LC}. The oscillator capacitance and inductance are denoted by C_{LC} and L respectively.

$$\hat{H}_{JC} = H_{LC} + H_{atom} + H_{int} \tag{2.34}$$

This interaction can be introduced into the circuit by coupling the qubit and oscillator capacitively, indicated in figure 2.5 (b) using the capacitance C_g. The energy of this interaction is given by[8]:

$$\hat{H}_{int} = C_g V_q V_{LC} = C_g \frac{Q_{qubit} Q_{LC}}{C_{qubit} C_{LC}}, \tag{2.35}$$

where V_q and V_{LC} are as shown in figure 2.2 (b). Writing this in terms of the raising and lowering operators yields

$$\hat{H}_{int} = -g(\hat{\sigma} - \hat{\sigma}^\dagger)(\hat{a} - \hat{a}^\dagger). \tag{2.36}$$

Similarly to 2.1.1 we can apply the rotating wave approximation and find the following final Hamiltonian.

$$\hat{H}_{JC} = \omega \hat{a}^\dagger \hat{a} - \frac{\omega_0}{2}\hat{\sigma}_z + g(\hat{a}^\dagger \hat{\sigma} + \hat{a}\hat{\sigma}^\dagger). \tag{2.37}$$

The only difference with 2.7 here is that g here is a real constant determined by circuit properties. For the remaining part of this paper, we will use 2.7 with the complex g. This so called "phase" of the interaction may also be engineered into a circuit, however, this is outside the scope of this paper as one needs a bit more advanced techniques to acquire this kind of control in the circuit. For a proper construction of such a circuit see [12].

2.2.2 Driving qubits

To use the full capabilites of qubits, complete control over the initialisation of its state is needed. This control of the qubit can be obtained by driving the qubit using a drive line and driving the qubit with a field as shown in figure 2.2 (a). In this paper, all the driving will be done using sinusoidal pulses with a square envelope. In this case the full Hamiltonian of the qubit during the driving is given as:

$$\hat{H}_{Drive} = -\frac{\omega_0}{2}\hat{\sigma}_z + iE\sin(w_d t - \theta)(\hat{\sigma} - \hat{\sigma}^\dagger). \tag{2.38}$$

Here w_d is the frequency of the drive, θ is the phase of the drive and E is the amplitude of the drive signal.// // If the driving frequency is sufficiently close to the qubit frequency and if the drive amplitude is sufficiently small to compared to the qubit frequency, one can apply the rotating wave approximation in a similar manner as was done in 2.1.1. This will yield:

$$\hat{H}_{Drive} = -\frac{\omega_0}{2}\hat{\sigma}_z + \frac{1}{2}E(e^{i\theta}e^{-i\omega_d t}\hat{\sigma}^\dagger + e^{-i\theta}e^{i\omega_d t}\hat{\sigma}). \tag{2.39}$$

Which, with the oscillator added, we will from now on write in the form:

$$\hat{H}_{Drive} = \omega\hat{a}^\dagger\hat{a} - \frac{\omega_0}{2}\hat{\sigma}_z + \varepsilon e^{-i\omega_d t}\hat{\sigma}^\dagger + \varepsilon^* e^{i\omega_d t}\hat{\sigma}, \tag{2.40}$$

where $\varepsilon = \frac{1}{2}Ee^{i\theta}$ is the complex drive amplitude.

To derive the time evolution of this Hamiltonian, since the oscillator and qubit are not interacting, it is easiest to first consider the qubit on its own. We first write the qubit part of the Hamiltonian in its matrix form:

$$\hat{H}_{drive} = \begin{pmatrix} -\frac{\omega_0}{2} & \varepsilon^* e^{i\omega_d t} \\ \varepsilon e^{-i\omega_d t} & \frac{\omega_0}{2} \end{pmatrix}. \tag{2.41}$$

Then to solve the complete time evolution of the system for some arbitrary state $|\psi\rangle = c_g(t)|g\rangle + c_e(t)|e\rangle$, one needs to solve the following differential equation:

$$\begin{pmatrix} i\dot{c}_g(t) \\ i\dot{c}_e(t) \end{pmatrix} = \begin{pmatrix} -\frac{\omega_0}{2} & \varepsilon^* e^{i\omega_d t} \\ \varepsilon e^{-i\omega_d t} & \frac{\omega_0}{2} \end{pmatrix} \begin{pmatrix} c_g(t) \\ c_e(t) \end{pmatrix} \tag{2.42}$$

To solve this, we will use the following ansatz:

$$\begin{pmatrix} c_g(t) \\ c_e(t) \end{pmatrix} = \begin{pmatrix} c_g(0)e^{-i(\frac{\Omega-\omega_d}{2})t} \\ c_e(0)e^{-i(\frac{\Omega+\omega_d}{2})t} \end{pmatrix}, \tag{2.43}$$

which when substituting it into 2.42 yields the following eigenvalue problem:

$$\Omega \begin{pmatrix} c_g(0) \\ c_e(0) \end{pmatrix} = \begin{pmatrix} -\Delta & 2\varepsilon^* \\ 2\varepsilon & \Delta \end{pmatrix} \begin{pmatrix} c_g(0) \\ c_e(0) \end{pmatrix}. \tag{2.44}$$

Here $\Delta = \omega_0 - \omega_d$. Solving this eigenvalues problem then gives the following eigenvalues

$$\Omega_\pm = \pm\sqrt{\Delta^2 + 4|\varepsilon|^2}. \tag{2.45}$$

Since these expressions are the same apart from a minus sign, we will from now on use just the expression

$$\Omega = \sqrt{\Delta^2 + 4|\varepsilon|^2} \tag{2.46}$$

and put in the minus sign where needed. Which correspond to the following (non normalized) eigenvectors:

$$\begin{aligned} |\psi_+\rangle &= \frac{1}{\sqrt{2}} \begin{pmatrix} e^{-i\theta}\frac{\sqrt{\Omega-\Delta}}{\sqrt{\Omega}} \\ \frac{\sqrt{\Omega+\Delta}}{\sqrt{\Omega}} \end{pmatrix} \\ |\psi_-\rangle &= \frac{1}{\sqrt{2}} \begin{pmatrix} -e^{-i\theta}\frac{\sqrt{\Omega+\Delta}}{\sqrt{\Omega}} \\ \frac{\sqrt{\Omega-\Delta}}{\sqrt{\Omega}} \end{pmatrix} \end{aligned} \tag{2.47}$$

And we can add in the earlier calculated time dependence

$$\begin{aligned} |\psi_+(t)\rangle &= \frac{1}{\sqrt{2}} \begin{pmatrix} e^{-i\theta}\frac{\sqrt{\Omega-\Delta}}{\sqrt{\Omega}} e^{-i\frac{\Omega-\omega_d}{2}t} \\ \frac{\sqrt{\Omega+\Delta}}{\sqrt{\Omega}} e^{-i\frac{\Omega+\omega_d}{2}t} \end{pmatrix} \\ |\psi_-(t)\rangle &= \frac{1}{\sqrt{2}} \begin{pmatrix} -e^{-i\theta}\frac{\sqrt{\Omega+\Delta}}{\sqrt{\Omega}} e^{-i\frac{-\Omega-\omega_d}{2}t} \\ \frac{\sqrt{\Omega-\Delta}}{\sqrt{\Omega}} e^{-i\frac{-\Omega+\omega_d}{2}t} \end{pmatrix} \end{aligned} \tag{2.48}$$

We can express $|e\rangle$ and $|g\rangle$ in terms of these eigenstates

$$\begin{aligned} |e\rangle &= \frac{\sqrt{\Omega+\Delta}}{\sqrt{2\Omega}}|\psi_+(0)\rangle + \frac{\sqrt{\Omega-\Delta}}{\sqrt{2\Omega}}|\psi_-(0)\rangle \\ |g\rangle &= e^{i\theta}\left(\frac{\sqrt{\Omega-\Delta}}{\sqrt{2\Omega}}|\psi_+(0)\rangle - \frac{\sqrt{\Omega+\Delta}}{\sqrt{2\Omega}}|\psi_-(0)\rangle\right) \end{aligned} \tag{2.49}$$

Then when starting with some arbitrary state $|\psi(0)\rangle = \alpha|g\rangle + \beta|e\rangle$ we can find the full time evolution of this state by first expressing this state in eigenstates using 2.49 and then evolving according to 2.48.

This will yield:

$$|\psi(t)\rangle = \alpha \begin{pmatrix} e^{i\frac{\omega_d}{2}t}\left(\cos\left(\frac{\Omega}{2}t\right) + i\frac{\Delta}{\Omega}\sin\left(\frac{\Omega}{2}t\right)\right) \\ -ie^{i\theta}e^{-i\frac{\omega_d}{2}t}\frac{\sqrt{\Omega^2-\Delta^2}}{\Omega}\sin\left(\frac{\Omega}{2}t\right) \end{pmatrix} + \beta \begin{pmatrix} -ie^{-i\theta}e^{i\frac{\omega_d}{2}t}\frac{\sqrt{\Omega^2-\Delta^2}}{\Omega}\sin\left(\frac{\Omega}{2}t\right) \\ e^{-i\frac{\omega_d}{2}t}\left(\cos\left(\frac{\Omega}{2}t\right) - i\frac{\Delta}{\Omega}\sin\left(\frac{\Omega}{2}t\right)\right) \end{pmatrix} \tag{2.50}$$

Using $|\psi\rangle(t) = \hat{U}(t) = |\psi(0)\rangle$, we then write down the full time evolution operator:

$$\hat{U}_{qubit}(t) = \begin{pmatrix} e^{i\frac{\omega_d}{2}t}\left(\cos\left(\frac{\Omega}{2}t\right) + i\frac{\Delta}{\Omega}\sin\left(\frac{\Omega}{2}t\right)\right) & -ie^{i\theta}e^{-i\frac{\omega_d}{2}t}\frac{\sqrt{\Omega^2-\Delta^2}}{\Omega}\sin\left(\frac{\Omega}{2}t\right) \\ -ie^{-i\theta}e^{i\frac{\omega_d}{2}t}\frac{\sqrt{\Omega^2-\Delta^2}}{\Omega}\sin\left(\frac{\Omega}{2}t\right) & e^{-i\frac{\omega_d}{2}t}\left(\cos\left(\frac{\Omega}{2}t\right) - i\frac{\Delta}{\Omega}\sin\left(\frac{\Omega}{2}t\right)\right) \end{pmatrix} \tag{2.51}$$

Very similar to the case in section 2.1.1, applying the drive to a qubit initially in some state, for example $|g\rangle$ will result in Rabi oscillations. Also, detuning has a similar effect on the population transfer as in the Jaynes-Cummings model, where the added detuning leads to only partial swaps between eigenstates. When the qubit starts in initial state $|e\rangle$, the excited state probability trace is nearly identical to figure 2.3 (a), only with a different frequency. The effects of the detuning will also produce a similar chevron pattern to the one in figure 2.3 (b). Since in the rest of this paper we are not interested in using these partial swaps, from now on we will always consider the drive to be in resonance with the qubit.

Adding in the time dependence of the oscillator is very easy as the separate Hamiltonians of the qubit and oscillator commute. Therefore the total time dependence is given as:

$$\begin{aligned} \hat{U}(t) = e^{-i(\hat{H}_{LC}+\hat{H}_Q)t} &= e^{-i\hat{H}_{LC}t}e^{-i\hat{H}_Q t} \\ &= e^{-i\omega\hat{a}^\dagger\hat{a}t}\hat{U}_{qubit}(t) \end{aligned} \tag{2.52}$$

2.2.3 Driving oscillators

Similar to driving qubits, it is also possible to drive (LC) oscillators. Just as with the qubit, this can be done by adding a drive line to the oscillator. Considering only the oscillator and a cosinusoidal drive with a square envelope, this will yield following Hamiltonian during the drive:

$$\hat{H}(t) = \omega \hat{a}^\dagger \hat{a} + iE\sin(\omega t - \theta)(\hat{a} - \hat{a}^\dagger) \tag{2.53}$$

Again, applying the rotating wave approximation yields a simplified Hamiltonian:

$$\hat{H}(t) = \omega \hat{a}^\dagger \hat{a} + \frac{E}{2}(e^{i\theta}e^{-i\omega_d t}\hat{a}^\dagger + e^{-i\theta}e^{i\omega_d t}\hat{a}) \tag{2.54}$$

For the oscillator drive, we will for now only consider the case that the oscillator and drive are in resonance, $\omega_d = \omega$. Going into the interaction picture with $\hat{H}_0 = \omega \hat{a}^\dagger \hat{a}$ and $\hat{H}_{int} = \frac{E}{2}(e^{i\theta}e^{-i\omega_d t}\hat{a}^\dagger + e^{-i\theta}e^{i\omega_d t}\hat{a})$ leads to

$$\hat{H}_{int,I}(t) = \frac{E}{2}(e^{i\theta}e^{-i\omega_d t}e^{i\omega t}\hat{a}^\dagger + e^{-i\theta}e^{i\omega_d t}e^{-i\omega t}\hat{a}) \tag{2.55}$$

Since we are considering the resonant case, this simplifies to

$$\hat{H}_{int,I} = \frac{E}{2}(e^{i\theta}\hat{a}^\dagger + e^{-i\theta}\hat{a}) \tag{2.56}$$

Since this Hamiltonian is time independent and $\hat{H}_0$ is also time independent, the time evolution operator of the interaction picture is given as:

$$\hat{U}_I(t) = e^{-i\hat{H}_{int,I}t} = e^{-i(\varepsilon\hat{a}^\dagger + \varepsilon^*\hat{a})t} = \hat{D}(-i\varepsilon t) \tag{2.57}$$

Applying a drive to a state is the same as displacing the state in the interaction picture.

Transforming back to the interaction picture yields

$$\hat{U}(t) = e^{-i\hat{H}_0 t}\hat{D}(-i\varepsilon t) \tag{2.58}$$

Which is just the displacement combined with a rotation around the origin of the “phase space". A more detailed explanation on the meaning of the displacement operator and phase space is given in section 2.4.1.

2.3 Derivation of the algorithm

The goal is to create arbitrary superpositions in an LC harmonic oscillator in the lab. To do this we will be using the physics of the Jaynes-Cummings model, as well as qubit driving to our advantage. We will use the qubit drive interactions to swap populations between the $|n, g\rangle$ and $|n, e\rangle$ states of the Jaynes-Cummings ladder and the Jaynes-Cummings interaction to swap between the $|n-1, e\rangle$ and $|n, g\rangle$ states.

2.3.1 General plan

A first important note is that we would like to start and end with our qubit and oscillator in disentangled states. Of course, if we start with the oscillator and qubit in the ground state, the first part of this will be met. $|\psi\rangle = |0\rangle \otimes |g\rangle$ For the second part, we would like to have our system in the following state, after applying the algorithm: $|\psi\rangle = (\sum a_n|n\rangle) \otimes |g\rangle$. Here the sum is the desired superposition state of the oscillator.

The process could be viewed as moving populations across the Jaynes-Cummings ladder. Using the Jaynes-Cummings interaction, populations can be moved between the $|n-1, e\rangle$ and $|n, g\rangle$ states of the ladder, where for each n, we found different Rabi frequencies. Using the qubit drive, populations can

be moved between the $|n, e\rangle$ and $|n, g\rangle$ states of the ladder. The Rabi frequency will be equal for all n since it only scales with the driving amplitude in this case, as shown in section 2.2.2. The Jaynes-Cummings interaction time propagations will be writtten as $\hat{C}_i$ and the qubit drive propgations as $\hat{Q}_i$. The i denotes the fact that this is the i'th operation on the system. In the end, we aim to construct a sequence of operations $\hat{U} = \hat{C}_n\hat{Q}_n...\hat{C}_2\hat{Q}_2\hat{C}_1\hat{Q}_1$ such that $(\sum a_n|n\rangle) \otimes |g\rangle = \hat{U}(|0\rangle \otimes |g\rangle)$.

The difficulty of creating an arbitrary superposition, is that every interaction effects all populated states. As an example, take the following state $(|1, g\rangle + |2, e\rangle)$. We want to move the population of the $|2, e\rangle$ state to the $|3, g\rangle$ state. We could do this by using the Jaynes-Cummings interation act for half of a Rabi cycle with frequency Ω_n. However since the $|1, g\rangle$ has a different Rabi frequency, it will perform a partial swap to the $|0, e\rangle$ state. Giving the following result: $\alpha|0, e\rangle + \beta|1, g\rangle + |3, g\rangle$ (neglecting some general phase factors). We see that in general, performing operations on the oscillator-qubit system, will influence all the populations of the states in different manners. (Although the operations on the qubit are a bit less problematic, different states will still get different phases).

Because of this it is quite difficult to find the correct operations by just trying to build the superpositions step by step from the ground state. Instead we will propose a different method, similar to [13]. Instead of finding a squence of operations to construct the desired state, we will first find a sequence of operation to deconstruct the desired state to the ground state and then, using the property that $\hat{U}(-t) = \hat{U}^\dagger(t)$, we will "flip" the sequence to find the desired construction sequence.

$$\begin{aligned} \hat{U}(-t) &= \hat{Q}_1^\dagger\hat{C}_1^\dagger\hat{Q}_2^\dagger\hat{C}_2^\dagger...\hat{Q}_n^\dagger\hat{C}_n^\dagger \\ \hat{U}(-t) &= \hat{U}^\dagger(t) \\ \hat{U}(t) &= \hat{C}_n\hat{Q}_n...\hat{C}_2\hat{Q}_2\hat{C}_1\hat{Q}_1 \end{aligned} \tag{2.59}$$

With each operation in the decomposition sequence, we will empty the highest populated state in the ladder, until we are left in the ground state of the total system. To do this we only need to consider the highest state and the state below it for the calculation of the correct operation, since each operation, qubit or Jaynes-Cummings will only let states interact in pairs. The reason this works, is that there will not be any states above the highest state that can randomly move around or interfere with the process, since all the states above the highest state are empty.

2.3.2 Calculation of the operation parameters

For our calculations, we will use interaction strength g with fixed amplitude and variable phase, and for the qubit drive, we will use a strength ε with fixed amplitude and variable phase, such that we can control the phase of the interactions. For both the Jaynes-Cummings interaction and qubit drive, we will be able to control the duration of the interaction, such that we can control how much population gets transferred during an interaction.

2.3.2.1 Calculation of Jaynes-Cummings parameters

As seen in 2.1, the time propagtor of the $|n-1, e\rangle$ and $|n, g\rangle$ states is given by the following matrix. (note that $|0, g\rangle$ is not included by these matrices since it does not interact using the jaynes-cummings interaction)

$$\hat{C}_{int,n}(t) = e^{-i(n-\frac{1}{2})\omega t}\begin{pmatrix} \cos(|g|\sqrt{n}t) & -ie^{i\theta}\sin(|g|\sqrt{n}t) \\ -ie^{-i\theta}\sin(|g|\sqrt{n}t) & \cos(|g|\sqrt{n}t) \end{pmatrix}, \tag{2.60}$$

where we used $g = |g|e^{i\theta}$ and $\hat{C}_{int,n}(t)$ denotes that this is the Jaynes-Cummings time propagation operator working on the $|n-1, e\rangle$ and $|n, g\rangle$ states subspace. Then, if we look at the highest populated states, we want $\alpha|n-1, e\rangle + \beta|n, g\rangle$ to go to $|n-1, e\rangle$. Hence we need to solve:

$$\hat{C}_{int,n}^\dagger(t)\begin{pmatrix}\alpha\\ \beta\end{pmatrix} = \begin{pmatrix} e^{i\phi} \\ 0 \end{pmatrix}, \tag{2.61}$$

where $e^{i\phi}$ is just some arbitrary left over phase. Since time propagation is a unitary operation and ϕ may be arbitrary, we only need to solve the following equation:

$$ie^{-i\theta}\sin\big(|g|\sqrt{n}t\big)\alpha+\cos\big(|g|\sqrt{n}t\big)\beta=0. \tag{2.62}$$

Which, if we choose the smallest value for t, has the following solution:

$$\begin{aligned} t &= \frac{\arctan(|\beta/\alpha|)}{|g|\sqrt{n}} \text{ if } \alpha\neq 0 \\ t &= \frac{\pi}{2|g|\sqrt{n}} \text{ if } \alpha = 0 \\ \theta &= \arg(\frac{\alpha}{i\beta}) \end{aligned} \tag{2.63}$$

2.3.2.2 Calculation of drive parameters

The calculation of the drive parameters follows similar arguments as for the Jaynes-Cummings parameters. The time propagator of states $|n,g\rangle$ and $|n,e\rangle$, as derived in 2.2, is now given by:

$$\hat{Q}_{int,n}(t)=e^{-in\omega t}\begin{pmatrix} e^{i\frac{w_d}{2}t}\cos(|\varepsilon|t) & -ie^{-i\theta}e^{i\frac{w_d}{2}t}\sin(|\varepsilon|t) \\ -ie^{i\theta}e^{-i\frac{w_d}{2}t}\sin(|\varepsilon|t) & e^{-i\frac{w_d}{2}t}\cos(|\varepsilon|t)\end{pmatrix}, \tag{2.64}$$

where we used $\varepsilon=|\varepsilon|e^{i\theta}$.

Now we want to go from $\alpha|n,g\rangle+\beta|n,e\rangle$ to $|n,g\rangle$ and thus we need to solve:

$$\hat{Q}^{\dagger}_{int,n}(t)\begin{pmatrix}\alpha\\ \beta\end{pmatrix}=\begin{pmatrix}e^{i\phi}\\ 0\end{pmatrix}, \tag{2.65}$$

with again ϕ some arbitrary phase. Using the same properties as before we get the equation:

$$ie^{i\theta}e^{-i\frac{\omega_d}{2}t}\sin(|\varepsilon|t)\alpha+e^{i\frac{\omega_d}{2}t}\cos(|\varepsilon|t)\beta=0. \tag{2.66}$$

Which leads to the following solution if we choose the smallest value for t: If $\alpha\neq 0$

$$\begin{aligned} t &= \frac{\arctan(|\beta/\alpha|)}{|\varepsilon|} \\ \theta &= \arg(\frac{i\beta e^{i\omega_d t}}{\alpha}) \end{aligned} \tag{2.67}$$

and if $\alpha=0$

$$\begin{aligned} t &= \frac{\pi}{2|\varepsilon|} \\ \theta &= 0 \end{aligned} \tag{2.68}$$

2.3.3 Further procedure

To calculate the full sequence of operations on the quantum system, we should alternate between the previously shown calculations, and also evolve the quantum system accordingly to those calculations, such that each calculations is performed on the correct quantum state. This should be done in the following manner.

1. Initialize

First select a desired final state $|\psi_{final}\rangle=(\sum a_n|n\rangle)\otimes|g\rangle$ with highest populated state N. Then set $|\psi_0\rangle=|\psi_{final}\rangle$

2. Calculate Jaynes-Cummings interaction

Now perform the calculation of 2.3.2.1 on $|\psi_0\rangle$. Then using the calculated parameters, calculate $\hat{C}_N^\dagger$. Then set $|\psi\rangle_1 = \hat{C}_N^\dagger|\psi_0\rangle$.

3. Calculate qubit drive

Perform the calculation described in 2.3.2.2 on $|\psi_1\rangle$. Using the calculated parameters, calculate $\hat{Q}_N^\dagger$. Then calculate $|\psi_2\rangle = \hat{Q}_N^\dagger|\psi_1\rangle$

4. Repeat

Repeat steps 2 and 3 by performing step 2 on the states $|\psi_{2k}\rangle$ and 3 on the states $|\psi_{2k+1}\rangle$ where k takes positive integer values. Repeat the steps until the state $|\psi_{2N}\rangle$ is reached. As a check, $|\psi_{2N}\rangle$ should be the ground state of the system.

5. Calculate final sequence

Using the the previously calculated parameters, now the sequence $\hat{U}(t) = \hat{C}_N\hat{Q}_N...\hat{C}_2\hat{Q}_2\hat{C}_1\hat{Q}_1$ may be calculated. Applying this sequence to the ground state of the system, will result in the desired final state.

2.4 Wigner Tomography

Being able to construct complex quantum states is only of use when you are also able to verify that you have in fact succeeded to create such a state. In this section we will explain how to describe and measure the created states in a LC oscillator. For this we first need some mathematical knowledge of the quantum phase space and Wigner functions. After that, the physical phenomena and mechanisms to measure the states will be explained.

2.4.1 Quantum phase space and the Wigner function

As shown in 2.2, the LC oscillator is completely analogous to the picture of a particle in a harmonic potential, with only some “renaming" of variables. Therefore we will show the properties of phase space for the oscillating particle. All the properties that we will discuss can then also be applied directly to the case of the LC-oscillator.

The state of a classical particle in a (1D) harmonic potential can be described by two variables, its position x and its momentum p. So the state of the particle at some time t can be described by the coordinates $(x(t), p(t))$. The space that consists of all possible particle states (x, p) is called the phase space. The path of the particle in this space described by $(x(t), p(t))$ is called its phase space trajectory. Phase space is a useful tool to look at the behaviour of systems. In the case of the particle in the harmonic potential, its phase space trajectory is an ellipse.

To also have a phase space representation in quantum mechanics, some changes have to be made. The exact path described by classical phase space is impossible in quantum mechanics due to the uncertainty principle. In the classical phase space, at every point in time, the position and momentum of the particle are exactly known. However, in quantum mechanics the position and momentum uncertainty of the particle have to obey $\Delta x \Delta p \geq \frac{\hbar}{2}$. Therefore instead of describing a state in phase space by a single point, the state should be described by some sort of unique phase space distribution function. There have been multiple attempts at creating such distributions, one of the most widely used ones is the Wigner distribution, which will also be used in this paper.

The Wigner function is defined as:

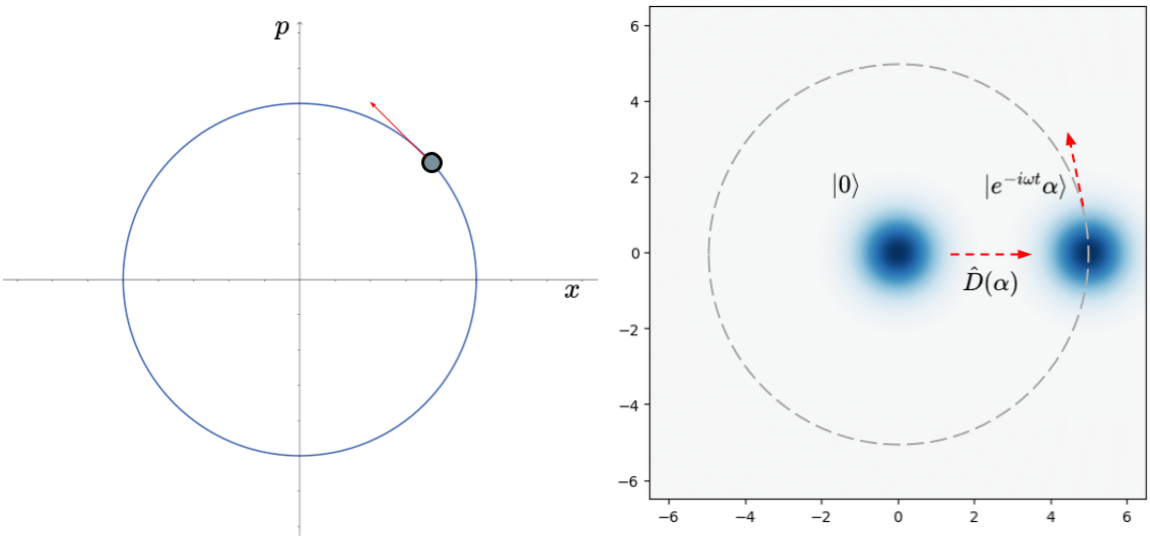

(a) (b)

Figure 2.6: (a) shows the classical phase space representation of an harmonic oscillator. The full behaviour of the system can be displayed using a connected curve, and the specific state at some time t may be indicated using one point. THe angular frequency of the motion is the frequency of the oscillator ω. (b) shows the quantum phase space representation. It shows the effects of the displacement operator $\hat{D}(\alpha)$ on the most basic coherent state $|0\rangle$, in this case transforming it to the state $|5\rangle$. The time behaviour of the displaced state is similar to that of the classical state as it will move in a circle as indicates. The state evolves as $|e^{-i\omega t}5\rangle$ with ω the oscillator frequency, which is again the angular frequency of the motion.

$$W(x,p) = \frac{1}{\hbar\pi}\int_{-\infty}^{+\infty} \psi^*(x+y)\psi(x-y)e^{\frac{2ipy}{\hbar}}dy \tag{2.69}$$

However, a experimentally easier form to use is:

$$W(\alpha) = \frac{2}{\pi}\langle\psi|\hat{D}^\dagger(-\alpha)\hat{\Pi}\hat{D}(-\alpha)|\psi\rangle, \tag{2.70}$$

which says that the value of the Wigner function at the complex point α in phase space is directly proportional to the expectation value of the parity operator at α. For a proof see [18]. Also note that instead of using two real valued coordinates, the Wigner function now takes one complex valued coordinate.

The Wigner function representation also works with density matrices, the parity representation is then:

$$W(\alpha) = \frac{2}{\pi}Tr[\hat{D}(-\alpha)\rho\hat{D}(\alpha)\hat{\Pi}] \tag{2.71}$$

Now we will note some properties.

For pure states, integrating over one of the two variables will yield the probability density function of the other variable:

$$|\psi(x)|^2 = \int_{-\infty}^{\infty} W(x,p)dp \tag{2.72}$$

and

$$|\varphi(p)|^2 = \int_{-\infty}^{\infty} W(x,p)dx \tag{2.73}$$

This makes it seem like the Wigner function is a joint probability distribution. However, this is not possible since this would mean that after performing a measurement on the system, we would now both x and p, which is again impossible due to the uncertainty principle. Instead of being positive, the Wigner function may also attain negative values. This negativity is typically a measure of how "non-classical" a state is. Loss effects such as decay and dephasing often have the effect of reducing the negativity of the Wigner function.

The so-called most classical state is the coherent state. Coherent states are defined as eigenstates of the annihilation operator:

$$\hat{a}|\alpha\rangle = \alpha|\alpha\rangle \tag{2.74}$$

The average photon number of such a state is given by

$$\langle\alpha|\hat{n}|\alpha\rangle = \langle\alpha|\hat{a}^\dagger\hat{a}|\alpha\rangle = |\alpha|^2 \tag{2.75}$$

The special thing about coherent states is that they are gaussians with the smallest possible uncertainty[19]. If you initially have a coherent state $|\psi(0)\rangle = |\alpha\rangle$. Then the time evolution is given as

$$|\psi(t)\rangle = |e^{-i\omega t}\alpha\rangle \tag{2.76}$$

[20] The state moves in circles, just as the classical oscillator state. These coherent states may also be written as[20]:

$$|\alpha\rangle = \hat{D}(\alpha)|0\rangle = e^{-\frac{|\alpha|^2}{2}} \sum_{n=0}^{\infty} \frac{\alpha^n}{\sqrt{n}}|n\rangle \tag{2.77}$$

Hence, using 2.2.3, we see that driving an oscillator from its ground state results in a coherent state.

2.4.2 The Rabi swap method

The results of section 2.1 and section 2.4.1 can be used in combination to create a procedure for physically measuring the Wigner function of a harmonic oscillator. In this paper the procedure will be described for circuits. However, the theory may be generalized to other systems with a similar Hamiltonian.

Instead of using a qubit to build a quantum state in an LC oscillator, a qubit will now be used to read out the oscillator. A system similar to 2.5 (b) will be used, which will again result in the system being described by the Jaynes-Cummings Hamiltonian 2.7. For the rest of this section, we will consider the interaction strength g to be real and positive, since for this procedure being able to control the phase of the interaction is not important. Initially the oscillator will be in an arbitrary state $|\psi_{LC}\rangle = (\sum a_n|n\rangle)$, from which we want to measure the Wigner functions. The qubit will always be initially in the ground state $|g\rangle$. The full initial state of the system may then be written as $|\psi\rangle = (\sum a_n|n\rangle) \otimes |g\rangle$. Evolving the system using the Jaynes-Cummings Hamiltonian will yield:

$$|\psi\rangle(t) = \hat{U}_{JC}(t)((\sum_{n\geq 0} a_n|n\rangle) \otimes |g\rangle), \tag{2.78}$$

where $\hat{U}_{JC}(t)$ is as in 2.22. Writing out the multiplication will yield:

$$|\psi(t)\rangle = a_0 e^{-i\frac{\omega}{2}t}|0,g\rangle + (\sum_{n\geq 1} a_n e^{-i\omega(n-\frac{1}{2})t}(\cos\big(g\sqrt{n}t\big)|n,g\rangle) - i\sin\big(g\sqrt{n}t\big)|n-1,e\rangle), \tag{2.79}$$

where g is real and positive. The excited state probability of the qubit at time t is then given by:

$$P_e(t) = |\langle\psi(t)|e\rangle|^2 = \sum_{n\geq 1} |a_n|^2 (\frac{1}{2} - \cos(2g\sqrt{n}t)). \tag{2.80}$$

This may be written in a more general form:

$$P_e(t) = \sum_{n\geq 1} |a_n|^2 P_{e,n}(t). \tag{2.81}$$

A very similar result may be found for the case where the initial oscillator state is described by a density matrix, as shown in the supplementary material of [6]. This will yield:

$$P_e(t) = \sum_{n\geq 1} p_n P_{e,n}(t), \tag{2.82}$$

where now p_n is the initial population of the $|n\rangle$ oscillator state.

For an harmonic oscillator, the Fock states are eigen states of the parity operator as there wave functions are symmetric or anti symmetric around the origin:

$$\hat{\Pi}|n\rangle = (-1)^n |n\rangle. \tag{2.83}$$

The expected parity of a (mixed) oscillator state ρ_{LC} will then be given by:

$$\langle\hat{\Pi}\rangle = Tr[\rho_{LC}\hat{\Pi}] = \sum_{n\geq 0} (-1)^n p_n, \tag{2.84}$$

where p_n are defined as before.

Since it is possible to measure the excited state probability trace of the qubit and if the functions $P_{e,n}(t)$ are known, it is possible to solve for the oscillator populations p_n using 2.82. Note that p_0 may be found using $p_0 = 1 - \sum_{n\geq 1}$. When decay and dephasing are also considered, the functions $P_{e,n}(t)$ are not the traces of individual Fock states anymore. Higher oscillator states may now influence the populations of lower oscillator states as their populations will decay and occupy lower states. This means that the trace $P_{e,n}(t)$ will be dependent on the initial oscillator state before the simulation. This state will be different for different points of the Wigner function since for different points the initial oscillator state from which the Wigner functions is measured is displaced by a different amount. As an approximation the form 2.82 may still be used, but now with $P_{e,n}(t)$ the traces of the qubit interaction with individual Fock states with decay and dephasing. Using these traces for $P_{e,n}(t)$, the values for p_n, the expected parity of the state may then be calculated using 2.84.

This gives the tools to calculate the Wigner function of the oscillator state, since the Wigner function, $W(\alpha)$ may be written in terms of the parity expectation of the oscillator state displaced by $\hat{D}(\alpha)$ as shown in 2.71. The procedure for calculating the Wigner function should then be the following,

1. Initialize

Prepare the initial state in the LC oscillator. The fit functions $P_{e,n}(t)$ should be simulated. In case there is decay and dephasing in the system, the functions $P_{e,n}(t)$ should be simulated using similar dephasing and decay. Alternatively, $P_{e,n}(t)$ may also be simulated without dephasing and decay is the decay and dephasing are low enough.

2. Displace

To calculate $W(\alpha)$, the initial oscillator state should be displaced by $-\alpha$, i.e. the operation $\hat{D}(\alpha)$ should be applied to the oscillator. This may be done using the theory from 2.2.3.

3. Measure the excited state trace

After displacing the state, the Jaynes-Cummings interaction with the qubit should be turned on and the qubit excited state trace should be measured during this time. The duration of the measurement

should be sufficiently long such that p_n may be calculated properly.

4. Calculate $W(\alpha)$

Using the qubit excited state probability trace and using 2.84, the expected parity at α may be calculated. With this expectation, $W(\alpha)$ can be calculated using 2.71.

5. Repeat

Steps 1, 2, 3 and 4 can be repeated using the same initial state preparation, but with a different value of α, such that the complete Wigner function of the oscillator state can be sampled.

Chapter 3

Method

In this chapter, we will discuss how we will test the physics and algorithms derived in chapter 2. To test the algorithms and to check calculations, we will use the QuTiP [21] python library to simulate the quantum systems and also as a handy tool for performing quantum mechanical calculations. It can simulate quantum systems using the Lindblad master equation[22][23] which will be used a lot to simulate loss effects in the quantum systems.

The functionality of the algorithm will first be demonstrated by simulating it. These simulations will also be used to visualize the workings and complexities of the algorithm. The simulations will also be used to study the effects of decay and dephasing on the results of the algorithm. This way we can get an idea of what the results of applying the algorithm in a practical system will be.

3.1 Testing and using state generation

The state generation algorithm has been programmed into Python using QuTiP. Simulation procedures and visualizing are also programmed using python. All the used algorithm and simulation functions have been put into a Jupyter Notebook[24] and can be found via [25]. However, to get an idea of how the simulations work and how to use it optimally, we will describe how the simulation procedure works and show which simulation parameters are important to get optimal results. After that, it will also be described how to perform more realistic simulations using Lindblad jump operators, such that decay and dephasing effects can be added to the simulation. In the last part of this section it will be shown how visualize and analyze the performed simulation to obtain the required results.

3.1.1 Simulation setup

To perform the correct simulation, the full simulation should be split into parts corresponding to the different operations performed on the system and the final state of each part of the simulations should be passed to the next simulation as the initial state. Then to simulate a sequence of the form $\hat{U}(t) = \hat{C}_n\hat{Q}_n...\hat{C}_2\hat{Q}_2\hat{C}_1\hat{Q}_1$, for each operator $\hat{C}_i$ the corresponding part of the simulation should be run using 2.7 as Hamiltonian, and the calculated parameters as interaction strength and duration of the simulation. For each operator $\hat{Q}_i$, the corresponding part of the simulation should be run using 2.40 as Hamiltonian, and again using the the calculated parameters as driving strength, duration and phase.

This procedure should again yield the desired final state, but now using the simulations tools, instead of using matrix multiplication. The individual simulation parts will be simulated using the QuTiP mesolve method [26]. The mesolve takes as input the initial state, the Hamiltonian to use for the system and a sequence of the steps for which it should evaluate the system state. The initial state input may either be a pure state vector or a density matrix. In the vector case the function will solve the Schrödinger equation and in the density matrix case, the Von Neumann equation[26].

There are also a few optional inputs for the mesolve functions. The first one is the so called "c_{ops}". This input may consists of a list of Lindblad collapse operators. If this list is nonempty, the mesolve

method will solve the Lindblad equation using the given collapse operators. The output of the mesolve method consists of an object which contains a list of the calculated system states at the time points that where put into the function. Alternatively, one can use the "$expt_{op}$s" input of the mesolve method to input a list of operators of which the expectation values should be evaluated at the input times. In this case the output of the mesolve method will consist of lists of the asked expectation values instead of the list of system states. The mesolve evaluates the requested values using an ODE solver. Which solver is used and options for the solver settings may be changed using the "Options" class in QuTiP [27]. Example code for solving a system with me solve is shown in C.6.

In the case of this thesis the state vector/matrix output of the mesolve method is always used as desired expectation values may also be calculated afterwards using the output states, full states are needed to calculate for example Wigner functions and the full states are needed to pass to the next part of the full simulation which uses a different Hamiltonian. The ODE solver used for the mesolve method in this paper is the default option "adams"[27]..

To get the correct simulation results, there are a few simulation settings that can drastically influence the quality of the simulation results. Firstly, for the best results, one should try to parametrize the frequencies. In the case of this paper, GHz was used as the unit of all frequencies. A second point that should be considered is the interaction strengths compared to the qubit frequency. If the interaction strengths are relatively low compared to the qubit frequency, the Rabi swap rates will be relatively low compared to the qubit and oscillator frequencies. Therefore, a relatively high number of timesteps and/or simulation steps is needed to capture the relatively fast dynamics of the qubit and oscillator during the relatively slow interactions. The difference between the timesteps and simulation steps is that the number of simulation steps is the number of steps the solver takes in between timesteps. The solver chooses this number dynamically. However, it is possible to increase the maximum allowed number of steps. This is sometimes needed, for example in the case described here, as the mesolve method may give a convergence error if the the maximum number of allowed steps is to small. The number of timesteps is equivalent to the number of time points at which the output states will be evaluated. Increasing this number will also allow the mesolve method to make more substeps per unit time.

Another useful parameter is the maximum step size. The mesolve method, dynamically chooses the step size such that it can use a larger step size if the differnece in the output of subsequent integration steps is small. However, when simulating with two different time scales, this can lead to problems. These can be solved by limiting the maximum step size and increasing the maximum number of simulation steps per input time step.

A third point is that the Hilbert space truncation should be chosen sufficiently large. This is especially important when dealing with displaced states and coherent states, since these can have a relatively high population in higher Fock states. Note that when working with higher number Fock states, the maximum frequencies in the simulation also increase. This should also be taken into consideration for choosing the right amount of simulation time steps.

To get a rough idea of which simulation settings are correct, some test simulation should be done without any dephasing or decay, since the theoretical behaviour of the system without dephasing and decay is known. Plotting expectation values of the total excitation, oscillator number and Qubit excitation will give a good indication of if the right parameters were chosen. In case wrong parameters are chosen, the plotted graphs will show a sort of "virtual" decay and dephasing while there should be none.

3.1.2 Performing simulations using the notebook

To use the state generation notebook, first the following system parameters have to be specified: qubit frequency (ω_0), Hilbert space size (N), interaction strength (g) and drive strength (ε) . If wanted, it is also possible to define decay and dephasing parameters for the qubit and/or oscillator. Lindblad collapse operators for these effects are already defined in the notebook. The notebook uses $\hbar = 1$ convention so all Hamiltonian's are in units of radial frequency (similar to in 2). Therefore all interaction strengths

should be in these units. Then to simulate a construction sequence the "simulate construction" function should be used. An example code cell using this function without any Lindblad collapse operators is shown in C.2.

The input of the function consists of the total requested state (oscillator state tensor product with qubit ground state), the maximum Fock number to which this state should be produced (normally just the highest occupied Fock state of the wanted oscillator state) and a list of Lindblad collapse operators (in this case an empty list). The “simulate construction" function will output the resulting states during the simulation and the corresponding time values. The given states are the total states in the combined oscillator-qubit Hilbert space, since the oscillator and qubit might be entangled during the sequence. The number of time steps, maximum number of simulation steps per time step and maximum simulation step size per operation of the sequence may be changed in the function definition. This is recommended to obtain optimal performance.

To simulate effects of dephasing and decay, one can simply add the corresponding Lindblad collapse operators in the function input as in C.3. The notebook already has qubit decay and dephasing and oscillator decay operators defined. However other Lindblad collapse operators may also be added in a similar manner to the already defined ones.

3.1.3 Analysis and visualization

To measure the quality of the obtained oscillator state at the end of the simulation, the fidelity of the final oscillator state will be calculated.

When the desired oscillator state is a pure state, $|\psi\rangle$, the fidelity is given by (reference)

$$F = \langle\psi|\rho|\psi\rangle = Tr[\rho|\psi\rangle\langle\psi|] \tag{3.1}$$

where ρ is the density matrix of the final state of the oscillator from the simulation. For the full fidelity definition see [28]. Intuitively, this measure may be viewed as the probability to measure desired state $|\psi\rangle$ from the final (mixed) state ρ.

For a given maximum populated state number, say N, the generation of the Fock state $|N\rangle$ takes the longest compared to other states with maximum populated state $|N\rangle$. However, they all take $2N$ operations to create. Therefore the generation sequence for the Fockstate will experience the largests effects of dephsaing and decay compared to other states with the same maximum state number. This means that calculating the fidelities of constructed Fock states will give a lower bound on the fidelities of all states with the same maximum state. This will be used to calculate the maximum producible state by a given physical system with given losses and a desired minimum fidelity.

Temporal behaviour of the process will be analyzed using time traces of the oscillator and qubit excitations, time evolution of the Wigner functions of the states during the simulation and the traces of the Fock state excitation's of the oscillator. A useful feature of qutip is that it has a build-in function for calculating Wigner functions of arbitrary quantum states.

3.2 Wigner tomography

Measuring the Wigner function of a produced state may be done using the Wigner tomography notebook. This notebook applies the Wigner tomography method described in section 2.4.2. This notebook will simulate the Wigner function measurement of an arbitrary initial state. With these simulations the effects of decay and dephasing on the measurement process can be tested.

3.2.1 Using the tomography notebook

As input parameters the notebook takes takes similar system parameters to the ones described in 3.1.2. Extra parameters are the produced Wigner image resolution and the Wigner image height. The Wigner image height determines the size of the phase space section for which values of the Wigner function will be calculated. The section is a square and a height value of for example 4 will result in a produced image where the real axis ranges from -2 to 2 and the imaginary axis also ranges from -2 to 2. The resolution parameter determines the amount of pixels or points in phase space the Wigner function will be calculates. A resolution of 30 will result in an evenly distributed $30x30$ grid on the selected phase space section.

To calculate the Wigner function at a point α, the procedure from 2.4.2 is followed. The initial oscillator state first gets displaced by multiplying it with the correct displacement operator. Then the excited state time trace $P_e(t)$ gets simulated using the mesolve method and the displaced initial state. The functions $P_{e,n}(t)$ are calculated by simulating single Fock states interacting with the qubit by the Jaynes-Cummings Hamiltonian. In this case the simulations are done without decay and dephasing. Since the traces gained from the simulation consist of discrete points, they are made continuous by using linear interpolation between the points. The number of simulation timesteps for the functions$P_{e,n}(t)$ is chosen to be significantly larger than the the number of simulation steps for $P_e(t)$. Therefore the interpolation should not result in problems.

The found functions are then used to fit the oscillator populations p_n using 2.82. The parameters are fit using the least squares function from the SciPy python library [29]. The found values for p_n are then used to calcluate the value of the Wigner functin using 2.84 and 2.71.

3.2.2 Choosing correct simulation settings

To get the best performance and output of the Tomography notebook, there are a couple of important setting that may be tweaked. These are the oscillator Hilbert space truncation size, duration of the $P_e(t)$ trace simulation and the type of simulation used to determine $P_{e,n}(t)$, i.e. the form of the fit functions.

When working without decay and dephasing in the $P_e(t)$ simulations, the most important parameters are the simulation simulation durations and the Hilbert space truncation size. Longer simulation durations will lead to better plots. These higher durations are also needed to distinguish between higher frequency oscillator states, as the traces of individual oscillator states $P_{e,n}(t)$ get more similar for larger values of n. This is because the frequency of the oscillations scale with $\sqrt{n}$, see section 2.1, hence the frequencies get more similar for higher n. This means that a longer simulation is needed to see significant differences in the different traces of the $P_{e,n}(t)$ functions. More difference in these functions will improve the fit.

The Hilbert space size should be taken large enough. This is of importance as for values of $W(\alpha)$ where $|\alpha|$ is large the initial state will get displaced more, which will result in more of the higher number oscillator states being populated. This can be sort of understood from equation 2.77. In principle, the Hilbert state truncation should be chosen just large enough such that the effects of the truncation fall outside the view of the produced Wigner image. To those this truncation a test option is added to the notebook. This test option will perform the same procedure as the simulation option, but instead of using simulations and fits to determine the value of the Wigner function at a point α, it will directly calculate 2.71 by using the build in functions in QuTiP for operator multiplication. The effects of the Hilbert space truncation will be very similar for both the test and simulation option. However, the test option runs a lot faster.

When decay and dephasing are added to the $P_e(t)$ simulation, the $P_{e,n}(t)$ functions may still be tried without dephasing and decay if the effects of the decay and dephasing are not very large over the time span of the trace $P_e(t)$. However, if this is not the case, the functions $P_{e,n}(t)$ should be simulated with

the same collapse operators that are used in the simulation for $P_e t$. To see which method is better, this thesis will compare both methods by looking at the produced Wigner functions. Choosing the correct simulation length will also improve the final produced Wigner function. Normally the duration should be as long as possible to better distinguish between higher order states. However, due to fact that the fit functions $P_{e,n}(t)$ are only approximations and do not model the system losses fully correctly, the fits may get worse for higher simulation durations. The simulation duration should therefore not be chosen to long. The correct simulation duration value is found using trial and error.

To improve the speed of the simulations and negate the effect of large time scale differences between the interaction rates and qubit and oscillator frequencies, the simulation Hamiltonian may be written in the interaction picture[16].

Chapter 4

Results and discussion

4.1 State Generation

Figure 4.1, 4.2 and 4.3 show that the algorithm works and can generate arbitrary states. Figure 4.1 shows the time traces of the oscillator and qubit photon number expectations, for the generation of the Fock state $|5\rangle$. The performed operations are shown in table B.1 of the appendix. The initial state of the system is $|0, g\rangle$ as can be seen from the expected values at $t = 0$. The final expected photon number is 5. This directly implies that the final oscillator state is $|5\rangle$ since the maximum number of added photons is 5 as can be seen from the 5 peaks in the qubit trace. It can also be seen that the qubit ends in $|g\rangle$ as wanted.

Figure 4.1 shows clearly how the different operations have different durations. In this case all qubit op-

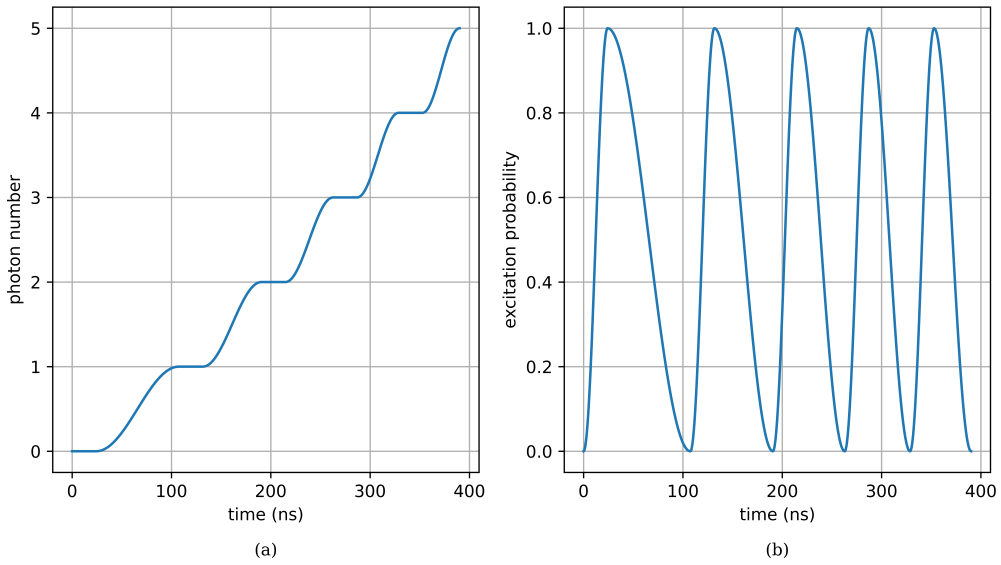

Figure 4.1: Construction simulation of the Fock state $|5\rangle$ without Lindblad operators, using parameters A.1. On the left the time trace of the oscillator photon number expectation. On the right the time trace of the qubit photon number expectation values

erations have the same duration since they are all so called "pi" swaps. The qubit operations correspond to the rising parts of the qubit trace. It can be seen that this duration is shorter than the durations of the Jaynes-Cummings operations. This is expected since the qubit drive strenth is significantly higher than the Jaynes-Cummings interaction strength and the swap frequencies are directly proportional to the interaction/drive strengths as shown in 2. (see A.1).

It can also be seen that the Jaynes-Cummings operations become shorter, while they are all "full swaps". This is because of the $\sqrt{n}$ factor in the Rabi frequency 2.1.2. Hence the swaps rates get higher for the swaps between the higher states. In general, figure 4.1 shows that for individual Fock states, the construction process consists of putting photons in the qubit using the drive, then swapping those photons to the oscillator and repeating this process.

Figure 4.2 shows why this view becomes more complex when generating states consisting of a superposition of Fock states. Figure 4.2 shows how the populations of the oscillator Fock states move during the production of the $|2\rangle + |5\rangle$ state. The calculated operation values are shown in table B.2 in the appendix. The figure shows the oscillator starting with all its population in its ground state and ending with all the population equally devided over the states $|2\rangle$ and $|5\rangle$. Since for superpositions of 2 Fock states the relative phase difference is not important, this indicates that the desired state is produced correctly.

The time segments with constant color indicate the qubit operations. Time segments with varying color indicate Jaynes-Cummings interactions. To generate the final state $|2\rangle + |5\rangle$, multiple different Focks states get populated at the same time using partial swaps, such that in the end the desired superposition is reached. This is illustrated by the light orange and yellow sections in figure 4.2. Some population is also transferred back down from 1 to 0, to later be moved up again. The reason this "spreading of populations" happens is because of the different Jaynes-Cummings Rabi frequencies between different oscillator levels. The different frequencies have the effect that for example applying a full swap between a state $|4, e\rangle \rightarrow |5, g\rangle$ will lead to a partial swap between any other states with some population. Hence as can be seen in 4.2 that the algorithm has to create correct populations in $|1, e\rangle$ and $|2, g\rangle$ such that a Jaynes-Cummings interaction with the duration of a full swap for the states $|4, e\rangle \rightarrow |5, g\rangle$ will lead to a correct partial swap such that $\alpha|1, e\rangle + \beta|2, g\rangle \rightarrow |2, g\rangle$. To create those partial populations, again specific partial swaps are needed. Thus from the first operation the algorithm needs to perform very specific swaps which depend on the swaps it needs to perform in the future. This is why instead of calculating the construction directly, the algorithm first calculates the deconstruction and then applies the time reversal as in 2.59.

When looking at 4.2 from right to left, it can be seen that to deconstruct the state, one only needs to swap the population from the highest state to the state below it. This may be a partial swap, but the correct swap only depends on the populations of $|n, g\rangle$ and $|n-1, e\rangle$ where n is the number of the highest populated state. This explains the method and calculation in 2.3.

Figure 4.3 shows the ability to control the relative phase between oscillator states by generating the states $|0\rangle + |1\rangle + |3\rangle$ and $|0\rangle + i|1\rangle + |3\rangle$. The blue ball in the first snapshot indicates that the initial oscillator state is its ground state. The final snapshot shows the produced final states, which correspond to the theoretically expected Wigner distributions.

Interestingly some of the Wigner functions of the in between snapshots, show very little negativity. This is a result of the fact that during this time of the procedure, the oscillator is entangled with the qubit. The qubit state used for the produced Wigner snapshot is the partial trace of the full entangled state. Tracing the qubit out of the full entangled state results in a mixed oscillator. The mixed states lead to less negativity in the Wigner function. For the final states, this is not a problem, since the oscillator and qubit should end in a disentangled state. The operations values for both sequences may be found in appendix table B.3 and B.4. Combining the results of figures 4.1, 4.2 and 4.3 shows the ability to generate arbitrary state since the ability to generate superpositions of multiple states as well as to control their relative phase is shown.

To test how well the algorithm will work for a system comparable to the one in our lab, simulations with decay and dephasing have been performed. The effects of oscillator and qubit decay and oscillator dephasing on the generation of the state $|5\rangle$ are shown in 4.4 where $T_1 = 700ns$ and $T_2 = 1\mu s$. For comparison a similar simulation to figure 4.1 is also shown. The final oscillator photon number expectation is 4.2 and the qubit final photon number is 0.1.

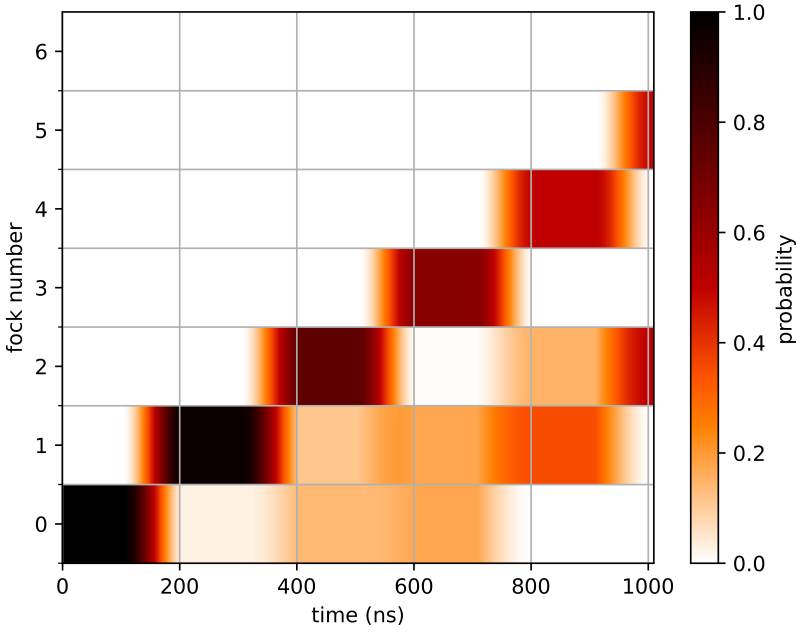

Figure 4.2: Construction simulation of $|2\rangle + |5\rangle$ without Lindblad operators, using parameters A.1. The image shows time trace of the Fock state populations of the oscillator during the simulation. The population is indicated using color where a darker color denotes a larger population as indicated by the colorbar. For each time step, the populations add up to 1.

The effects of decay and dephasing are quite significant as can be seen in 4.4. The expected photon number of the oscillator is close to 1 lower than the desired photon number. An explanation for the large effect of the dephasing and decay may be that the performed operations are calculated for a system without losses. The losses of the system lead to the operations being applied to different initial states than they where intended to. This may result in an output state that is slightly more different from the intended output state. Then again an operator will be applied to an incorrect state, and the errors will add up. However, it is not clear how much of the final error is due to the algorithm being applied to incorrect states and how much of the error is just the effect of the decay on its own. The interactions between the qubit and oscillator will also create larger decay effects on the oscillator than the oscillator on its own would have since the states of the oscillator are via the Jaynes-Cummings interaction, influenced by the errors of the qubit state due to the dephasing and decay of the qubit.

The qubit trace of 4.4 shows that the decay and dephasing also make the qubit end up out of the desired ground state. This should be be a better measure of the errors of the algorithm made by incorrect initial states. This is because there are no "creation" Lindeblad operators in the simulation, so no photons are added to the system apart from the drive. Therefor over time the qubit is expected to decay to its groundstate. Therefor the qubit not being in its groundstate should be a direct result of the error effects of the algorithm. This could be investigated further. The qubit not being in its groundstate may also indicate that it is still slightly entangled with the oscillator, which is undesired.

To get a measure of the effect of the decay and dephasing on the final result of state generation and how improvements in the lab system will improve the result, simulations for Fock states $|n\rangle$ for $1 \leq n \leq 9$ have been performed and for each simulation the fidelity of the final state with the desired state had been calculated. The baseline system values used are shown in table A.3.

Two sequences of simulations have been performed. Figure 4.5 (a) shows the effects of improving

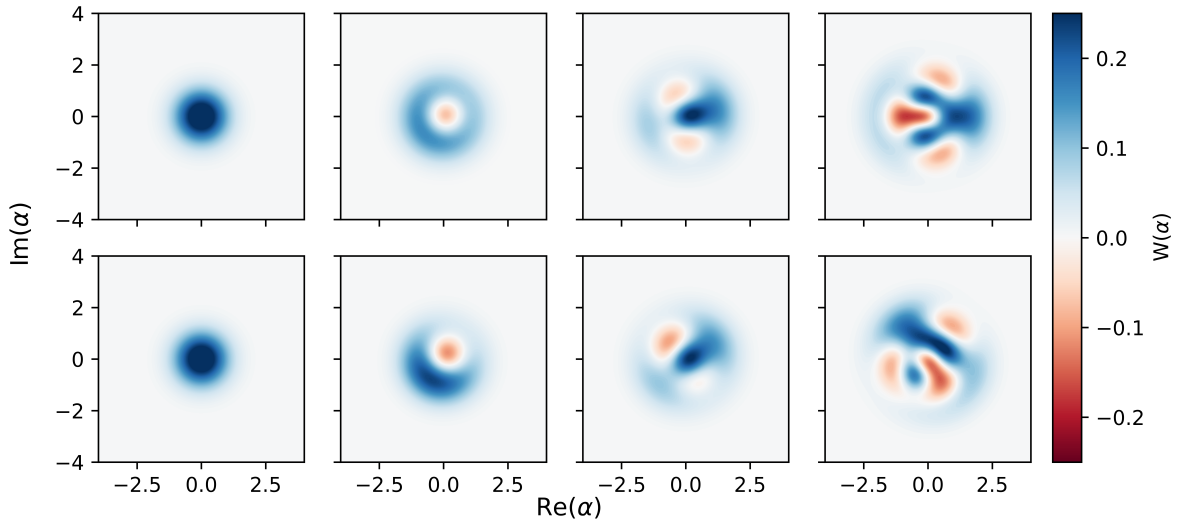

Figure 4.3: Construction sequences of $|0\rangle + |1\rangle + |3\rangle$ (upper) and $|0\rangle + i|1\rangle + |3\rangle$ (lower) . The shown Wigner functions are snapshots of the oscillator state during the construction sequence at times: $t = 0ns$, $t = 76ns$, $t = 135ns$ and the final state. Which are at $t = 197ns$ and at $t = 200ns$ for the upper and lower sequence respectively. The left most images show the oscillator in the ground state and the right most images show the produced final state. The images in between show the Wigner functions after 2 and 4 operations have been performed (the final is after 6 operations)

T_2. $T_2 = 250ns$ is the experimentally measured value of the current lab system. However, the value such that the Rabi oscillation measurements for T_2 match the simulated Rabi oscillations is $T_2 = 1\mu s$. The discrepancy between the two values has not yet been resolved, hence the effects of both are shown as it is not yet clear which value of T_2 would be correct for the state production. $T_2 = 1.4\mu s$ is the theoretically optimal value for T_2 given $T_1 = 700ns$. It can be seen in figure 4.5 (a) that the experimentally measured value of T_2 gives a result reasonably close to the optimal values.

Figure 4.5 (b) shows the effects of improving T_1 and κ. Here T_2 is changed accordingly such that Γ_ϕ remains the same for the different simulations. The blue plot in 4.5 again shows the results of the current system (parameters A.3). An improved system has been designed. The orange plot shows the effect of the the oscillator losses. $\kappa = 60kHz$ is the expected improved value. This is a conservative guess on the improved value as it has not been measured yet. The green plot shows the effect of the improved qubit, where now $T_1 = 3\mu s$. However, this values has yet to be measured experimentally and is only an estimation. 4.5 shows that the final state fidelity's seem to be limited by the qubit T_1, since the values of the current system and system with improved oscillator are very similar.

In both (a) and (b) of 4.5 fidelities decrease for a increasing number Fock state. This is partially expected as the sequence duration becomes longer for the production of higher number states. This longer duration will lead to larger effects of decay and dephasing in the final state. Again, it is unknown how large the effect of applying the sequence operations to wrong initial states is in the reduced final fidelities.

As stated a few times before, future research could be done on how large the error of the algorithm is due to incorrect initial states and if there would be ways to compensate for the incorrect initial states in the calculation of the algorithm.

An other way to increase to final state fidelity would be to increase the Qubit drive strength (ε) and Jaynes-Cummings coupling strength (g). This would shorten the operation durations and would decrease the effects of decay and dephasing on the procedure. Further research could be done to investigate if increasing coupling and interaction strength or improving T_2 and T_1 would lead to further

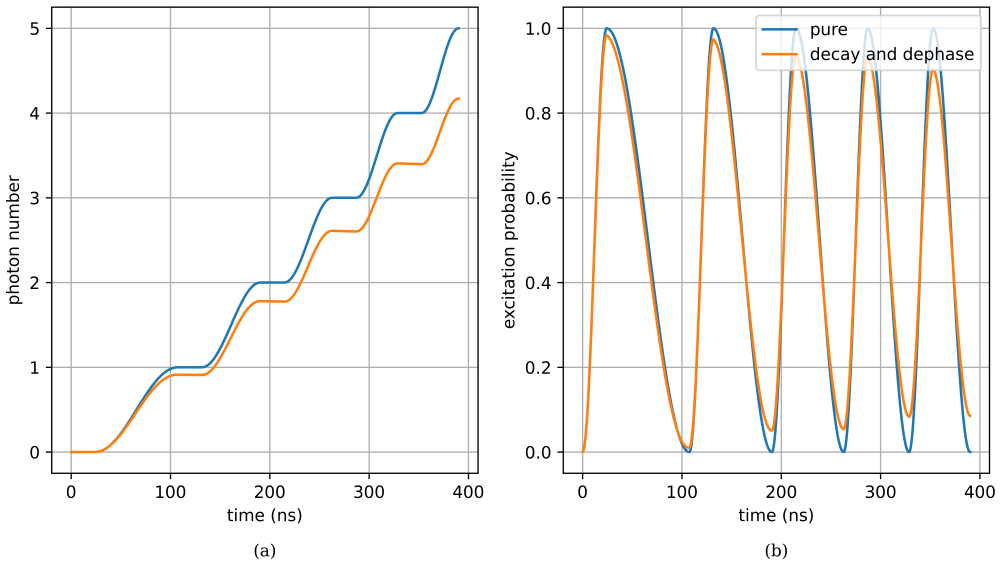

Figure 4.4: Construction simulation of $|5\rangle$ with and without Lindblad operators for qubit and oscillator decay and qubit dephasing, using parameters A.3. The left graph shows the oscillator photon number expectation and the right graph the qubit photon number expectation. In both graphs, the traces for the simulations with and without Lindblad operators are shown for comparison.

improvements in the final state fidelity.

4.2 Tomography

To examine the effects of the decay and dephasing of the lab system on the Wigner tomography, three simulated Wigner functions of the cat-state $|\alpha = 2\rangle + |\alpha = -2\rangle$ are shown in figure 4.6. Figure 4.6 (a) and (d) show the Wigner simulated without any loss effects. Figure 4.6 (b) and (e) show the Wigner functions simulated with Lindblad collapse operators but without collapse operators in the fit functions $P_{e,n}(t)$(see section 2.4.2). Figure 4.6 (c) and (f) show the Wigner function simulated with collapse operators in both the simulation and fit functions. In the simulations of figure 4.6 (a), (b) and (c), the simulations for $P_e(t)$ where run for a duration $t = 400ns$. In 4.6 (d), (e) and (f) they were run for $t = 800ns$. All six simulations are run using the same Hilbert space truncation,$N = 40$. Plots (a) and (d) where used as benchmarks to compare (b-c) and (e-f) to.

It can be seen from figure 4.6 that increasing the trace duration for $P_e(t)$ significantly improves the produced Wigner functions. Figure 4.6 (a) to (d) and (c) to (f) show that the improvements of the results are larger for points where $|\alpha|$ is larger. This is expected, since for measuring points of the Wigner function with a larger displacement the initial state that we want to measure gets displaced more. When expanding a quantum state in the Fock state basis, points in phase space further away from the origin generally are influenced more by higher order Fock states in the expansion of the quantum state. This may intuitively be sort of understood by looking at the expansion of a coherent state, see equation 2.77. The expansion shows that for higher values of $|\alpha|$, i.e. a further displaced state, higher order Fock state terms in the expansion get more dominant. As states earlier in section 3.2.1, distinguishing between higher order Fock states is more difficult with a shorter simulation duration. This will lead to more error in fits for further displaced points in the Wigner functions as the higher order Fock state traces are more important here. The red vertical curves that are visible in figures 4.6 (a), (b) and (c) are artifacts that seem to be the result of the described higher state errors. For higher simulation duration they move outward, since the Wigner reconstruction is more precise for higher order states with the higher duration. For $t = 800ns$, they have completely moved out of the field of view of the image for 4.6 (d) and (f)

Figure 4.6 (b) and (c) and figure C.4 (e) and (f) show clear differences between the results of the

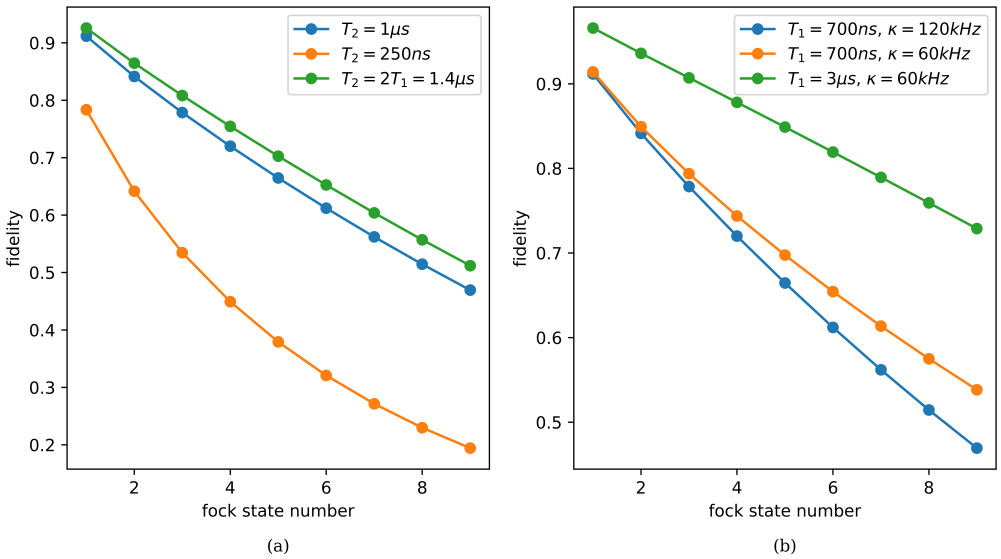

Figure 4.5: Graphs of final produced state fidelity for different Fock states $|n\rangle$. In (a) the values of T_2 has been varied with $T_1 = 700ns$ and $\kappa = 120kHz$. $T_2 = 250ns$ is the experimentally measured vale, $T_2 = 1\mu s$ is the value for which experimentally measured Rabi oscillations match the simulated ones and $T_2 = 1.4\mu s$ is the highest possible value given T_1. (b) shows a similar graph, but now with T_1 and κ varied instead. Here T_2 was chosen such that Γ_ϕ remains constant. The blue graph again indicates the lab system with current system values. The orange graph shows the fidelity's for an improved $\kappa = 60kHz$. The green graph shows the graph for a system where both $T_1 = 3\mu s$ and $\kappa = 60kHz$ are improved with respect to the current values.

fit functions $P_{e,n}(t)$ with and without decay and dephasing. Figure 4.6 (c) and (f) show that the fit method with decay and dephasing produce results very similar to those of the benchmark tests. For $t = 400ns$, they are nearly identical in the center parts of the image, which show the interference pattern of the cat state. For $t = 800ms$, they are indistinguishable by the eye. Figure 4.6 (b) shows that for the shorter duration the method without decay in the fit functions is influenced a lot by the decay and dephasing in the simulation. The interference pattern is similar but less nuanced to the ones shown in figure 4.6 (a) and (c). However, the method also shows large differences in the produced image (b) with the other two methods, such as the large negative areas in the image. The method does show an improved image in 4.6 (e), where the large negative areas have faded away and only some artifacts around the edges remain. However, the negativity and positivity of the interference pattern in 4.6 (e) are less defined than in 4.6 (d) and (f). The decreased contrast in the interference pattern seems to resemble the effects of decoherence on a cat-state, where also the interference pattern will vanish and results in a mixed state. This may be a consequence of the fact that to compensate for the fact that the fit function $P_{e,n}(t)$ do not include decay, the fit chooses smaller values for p_n to still try to match the decay of the simulated trace $P_e(t)$, a sort of averaging procedure.

The method of using decay and dephasing in the fit functions produces a more similar results to the benchmark method compared to the method using fit functions without dephasing and decay for shorter simulation durations. The method of fit functions without decay and dephasing could be made more precise be using longer simulation durations for $P_e(t)$, however, this may result in the produced Wigner function showing even less negativity and coherence.

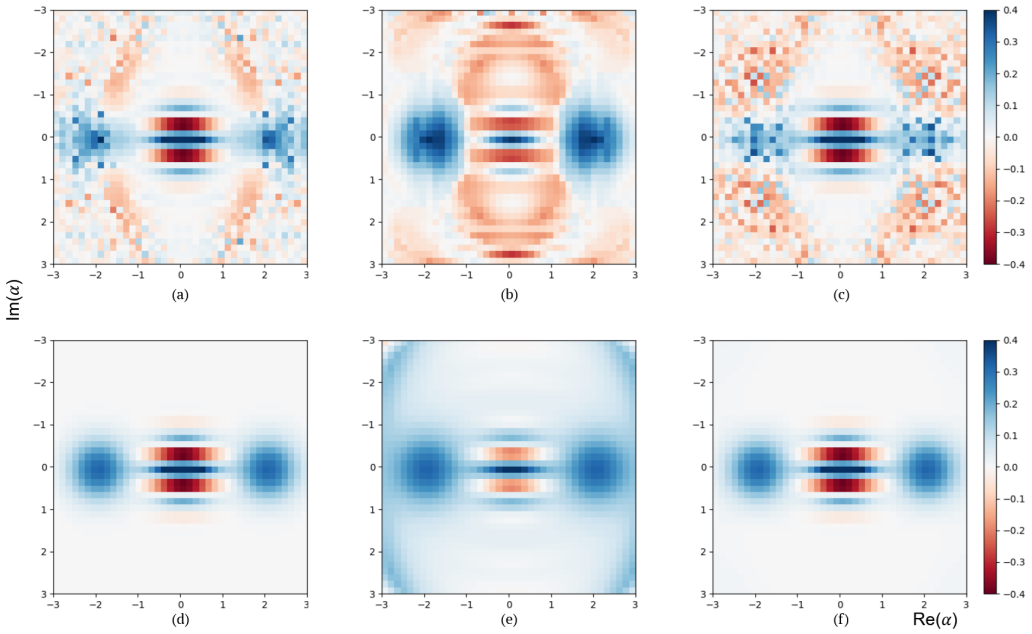

Figure 4.6: Images of simulated Wigner functions of the cat-state $|\alpha = 2\rangle + |\alpha = -2\rangle$ for 2 simulation durations. In (a) and (d) the simulation is done without any decay and dephasing, in (b) and (e) the simulation is done with dephasing and decay and in (c) and (f) both the simulation and the fit functions have decay and dephasing. In (a), (b) and (c) the simulation duration for $P_e(t)$ is $t = 400ns$. In (d), (e) and (f), the simulation duration for $P_e(t)$ is $t = 800ns$.

Chapter 5

Conclusion

In this paper, protocols for generating arbitrary states in an LC-oscillator using a Jaynes-Cummings type of interaction and for measuring them were derived. The protocol for state generation was tested using simulations and the results of the simulations have been used to give more insight in the inner workings of the algorithm. It was shown that the algorithm was capable of producing superpositions of multiple Fockstates as well as having full control over the relative phase differences between the states in the superposition.

The real word limits of the system have also been tested by using Lindblad operators in the simulation, similar to the real world setup. It was found that the loss effects had a significant impact on the fidelity of the produced state. However, it was not clear how much of the error in the final state is due to the inevitable decay and dephasing effects, and how much of the error is due to the operations in the algorithm being applied to incorrect states. This could be investigated further. It was also proposed that to improve the final state fidelity, the interaction strength could be increased such that the durations of the operations are shorter.

The protocol for measuring Wigner functions was also derived and tested using simulations and the lab system parameter values. Three kinds of simulations where done: without decay and dephasing, with decay and dephasing for the simulation only and with decay and dephasing for both the the simulation and fit functions. The simulation without decay and dephasing was used as a benchmark to compare the other two to. Both simulations with and without decay in the fit functions gave good results for the Wigner function when using a longer simulation duration. However for shorter simulation duration, $t = 400ns$, the method with decay in the fit functions was more successful. For the longer simulation duration $t = 800ns$, the method with out decay in the fit functions also showed a less pronounced interference pattern. Considering these results, the method using decay and dephasing in the fit functions was recommended.

Bibliography

[1] Mario F. Gely and Gary A. Steele. "Superconducting electro-mechanics to test Diósi–Penrose effects of general relativity in massive superpositions". In: *AVS Quantum Science* 3.3 (Sept. 2021), p. 035601. ISSN: 2639-0213. DOI: 10.1116/5.0050988. eprint: https://pubs.aip.org/avs/aqs/article-pdf/doi/10.1116/5.0050988/19738649/035601_1_online.pdf. URL: https://doi.org/10.1116/5.0050988.

[2] Igor Pikovski et al. "Probing Planck-scale physics with quantum optics". In: *Nature Physics* 8.5 (Mar. 2012), pp. 393–397. ISSN: 1745-2481. DOI: 10.1038/nphys2262. URL: http://dx.doi.org/10.1038/nphys2262.

[3] Amarendra K. Sarma and Sampreet Kalita. *Tutorial: Cavity Quantum Optomechanics*. 2022. arXiv: 2211.02596.

[4] Eyob A. Sete and H. Eleuch. "High-efficiency quantum state transfer and quantum memory using a mechanical oscillator". In: *Physical Review A* 91.3 (Mar. 2015). ISSN: 1094-1622. DOI: 10.1103/physreva.91.032309. URL: http://dx.doi.org/10.1103/PhysRevA.91.032309.

[5] C A Regal and K W Lehnert. "From cavity electromechanics to cavity optomechanics". In: *Journal of Physics: Conference Series* 264 (Jan. 2011), p. 012025. ISSN: 1742-6596. DOI: 10.1088/1742-6596/264/1/012025. URL: http://dx.doi.org/10.1088/1742-6596/264/1/012025.

[6] Max Hofheinz et al. "Synthesizing Arbitrary Quantum States in a Superconducting Resonator". In: *Nature* 459.7246 (2009), pp. 546–549. DOI: 10.1038/nature08005.

[7] Thomas E. Roth, Ruichao Ma, and Weng C. Chew. "The Transmon Qubit for Electromagnetics Engineers: An introduction". In: *IEEE Antennas and Propagation Magazine* 65.2 (Apr. 2023), pp. 8–20. ISSN: 1558-4143. DOI: 10.1109/map.2022.3176593. URL: http://dx.doi.org/10.1109/MAP.2022.3176593.

[8] P. Krantz et al. "A quantum engineer's guide to superconducting qubits". In: *Applied Physics Reviews* 6.2 (June 2019). ISSN: 1931-9401. DOI: 10.1063/1.5089550. URL: http://dx.doi.org/10.1063/1.5089550.

[9] Uri Vool and Michel Devoret. "Introduction to quantum electromagnetic circuits". In: *International Journal of Circuit Theory and Applications* 45.7 (June 2017), pp. 897–934. ISSN: 1097-007X. DOI: 10.1002/cta.2359. URL: http://dx.doi.org/10.1002/cta.2359.

[10] Christopher Gerry and Peter Knight. *Introductory Quantum Optics*. Cambridge, UK: Cambridge University Press, 2005. ISBN: 9780521527354.

[11] Susanne Richer and David DiVincenzo. "Circuit design implementing longitudinal coupling: A scalable scheme for superconducting qubits". In: *Physical Review B* 93.13 (Apr. 2016). ISSN: 2469-9969. DOI: 10.1103/physrevb.93.134501. URL: http://dx.doi.org/10.1103/PhysRevB.93.134501.

[12] C.A. Potts et al. "Photon-Pressure Circuit Quantum Electrodynamics (in preparation)". In: ().

[13] C.K. Law and J.H. Eberly. "Arbitrary control of a quantum electromagnetic field". In: *Physical Review Letters* 76.2 (1996), pp. 1055–1058. DOI: 10.1103/physrevlett.76.1055.

[14] Yiwen Chu et al. "Creation and control of multi-phonon Fock states in a bulk acoustic-wave resonator". In: *Nature* 563.7733 (Nov. 2018), pp. 666–670. ISSN: 1476-4687. DOI: 10.1038/s41586-018-0717-7. URL: http://dx.doi.org/10.1038/s41586-018-0717-7.

[15] A. Ben-Kish et al. “Experimental demonstration of a technique to generate arbitrary quantum superposition states”. In: *Physical Review Letters* 90.3 (2003). DOI: doi:10.1103/physrevlett.90.037902.

[16] Ramamurti Shankar. *Principles of Quantum Mechanics*. 2nd. Springer, 1994.

[17] N. B. Kopnin. *Introduction to The Theory of Superconductivity*. Helsinki University of Technology, 2009.

[18] Antoine Royer. “Wigner function as the expectation value of a parity operator”. In: *Phys. Rev. A* 15 (2 Feb. 1977), pp. 449–450. DOI: 10.1103/PhysRevA.15.449. URL: https://link.aps.org/doi/10.1103/PhysRevA.15.449.

[19] *Lecture 4: Quantum fluctuations, the quantum harmonic oscillator, and coherent states*. https://qsm.quantumtinkerer.tudelft.nl/4_ZPFs/. [Accessed 19-06-2024]. 2024.

[20] David Tong. *David Tong: Applications of Quantum Mechanics — damtp.cam.ac.uk*. http://www.damtp.cam.ac.uk/user/tong/aqm.html. [Accessed 13-06-2024]. 2017.

[21] J.R. Johansson, P.D. Nation, and Franco Nori. “QuTiP 2: A Python framework for the dynamics of open quantum systems”. In: *Computer Physics Communications* 184.4 (Apr. 2013), pp. 1234–1240. ISSN: 0010-4655. DOI: 10.1016/j.cpc.2012.11.019. URL: http://dx.doi.org/10.1016/j.cpc.2012.11.019.

[22] Daniel Manzano. “A short introduction to the Lindblad master equation”. In: *AIP Advances* 10.2 (Feb. 2020). ISSN: 2158-3226. DOI: 10.1063/1.5115323. URL: http://dx.doi.org/10.1063/1.5115323.

[23] Klaus Mølmer, Yvan Castin, and Jean Dalibard. “Monte Carlo wave-function method in quantum optics”. In: *J. Opt. Soc. Am. B* 10.3 (Mar. 1993), pp. 524–538. URL: https://opg.optica.org/josab/abstract.cfm?URI=josab-10-3-524.

[24] Thomas Kluyver et al. “Jupyter Notebooks – a publishing format for reproducible computational workflows”. In: *Positioning and Power in Academic Publishing: Players, Agents and Agendas*. Ed. by F. Loizides and B. Schmidt. IOS Press. 2016, pp. 87–90.

[25] *Bep Marijn Morssink*. https://gitlab.tudelft.nl/steelelab/bep-marijn-morssink/. [Accessed 13-06-2024]. 2024.

[26] J.R. Johansson, P.D. Nation, and Franco Nori. “QuTiP: An open-source Python framework for the dynamics of open quantum systems”. In: *Computer Physics Communications* 183.8 (Aug. 2012), pp. 1760–1772. ISSN: 0010-4655. DOI: 10.1016/j.cpc.2012.02.021. URL: http://dx.doi.org/10.1016/j.cpc.2012.02.021.

[27] *Setting Options for the Dynamics Solvers*. https://qutip.readthedocs.io/en/qutip-4.7.x/guide/dynamics/dynamics-options.html. [Accessed 13-06-2024]. 2024.

[28] Richard Jozsa. “Fidelity for Mixed Quantum States”. In: *Journal of Modern Optics* 41.12 (1994), pp. 2315–2323. DOI: 10.1080/09500349414552171. eprint: https://doi.org/10.1080/09500349414552171. URL: https://doi.org/10.1080/09500349414552171.

[29] Pauli Virtanen et al. “SciPy 1.0: Fundamental Algorithms for Scientific Computing in Python”. In: *Nature Methods* 17 (2020), pp. 261–272. DOI: 10.1038/s41592-019-0686-2.

Appendix A

Lists of use parameter values

This section of the appendix contains tables with parameter values used for the simulations.

Table A.1: Table of settings for state generation without Lindblad collapse operators.

Parameter	Value
ω	6.1 GHz
ω_0	6.1 GHz
ω_d	6.1 GHz
$\|g\|$	$3 * 10^{-3}$ GHz
$\|\varepsilon\|$	$64 * 10^{-3}$ GHz

Table A.2: Table of the solver settings. N indicates the oscillator Hilbert space size, num time steps the number of simulation time steps per operation, max step size the maximum step size taken by the solver and max num steps the maximum number of steps taken by the solver in between the input time steps

N	15
num time steps	101
max step size	10^{-3} ns
max num steps	2500
ODE solver	adams

Table A.3: Table with the lab system values.

Parameter	Value
ω	6.1 GHz
ω_0	6.1 GHz
ω_d	6.1 GHz
$\|g\|$	$3 * 10^{-3}$ GHz
$\|\varepsilon\|$	$64 * 10^{-3}$ GHz
T_1	700 ns
T_2	$1\mu s$
κ	120 GHz

Appendix B

Operation sequences

This part of the appendix contains operation sequences calculated for the simulations in section 4.

Table B.1: Operation sequence duration and phase values for the state $|5\rangle$. The operations are labeled Q for a qubit operation and C for a Jaynes-Cummings operation and are showed in order.

Operation	Duration (ns)	Phase (rad)
Q_1	24	0
C_1	83	0
Q_2	24	0
C_2	59	3.14
Q_3	24	0
C_3	48	0
Q_4	24	0
C_4	42	0
Q_5	24	0
C_5	37	0

Table B.2: Operation sequence duration and phase values for the state $|2\rangle + |5\rangle$. The operations are labeled Q for a qubit operation and C for a Jaynes-Cummings operation and are showed in order.

Operation	Duration (ns)	Phase (rad)
Q_1	24	1.35
C_1	75	-2.93
Q_2	17	-1.74
C_2	51	-2.97
Q_3	18	-2.93
C_3	47	-3.14
Q_4	17	1.94
C_4	42	0
Q_5	24	0
C_5	37	0

Table B.3: Operation sequence duration and phase values for the state $|0\rangle + |1\rangle + |3\rangle$. The operations are labeled Q for a qubit operation and C for a Jaynes-Cummings operation and are showed in order.

Operation	Duration (ns)	Phase (rad)
Q_1	22	1.10
C_1	48	1.26
Q_2	16	0.47
C_2	38	-1.88
Q_3	24	0
C_3	48	0

Table B.4: Operation sequence duration and phase values for the state $|0\rangle + i|1\rangle + |3\rangle$. The operations are labeled Q for a qubit operation and C for a Jaynes-Cummings operation and are showed in order.

Operation	Duration (ns)	Phase (rad)
Q_1	17	-1.78
C_1	56	1.75
Q_2	16	-2.67
C_2	38	-0.31
Q_3	24	0
C_3	48	0

Appendix C

Code

This section of the appendix contain simple examples of the notebook setup and simulations.

C.1 Code setup

```
N = 15
#using units of Ghz and ns

w = 6.1 * 2*np.pi #oscillator angular frequency
w0 = 6.1 * 2*np.pi #qubit angular frequency
wd = 6.1 * 2*np.pi #drive angular frequency

g = 3*10**-3 * 2*np.pi #Jaynes-Cummings interaction strength
l = 65*10**-3 #drive amplitude
#Setting T1,T2 and oscillator decay kappa
T1 = 700  #700ns
rate_1 = 1/T1
T2 = 1*10**3 #1mus
rate_phase = 1/T2-0.5*rate_1
kappa = 120*10**-6

#Setting solver options

options=Options(max_step=1e-3,nsteps=2500)

#Defining anihilation operators and pauli z matrix in tensored Hilbert space

a = qutip.tensor(qutip.destroy(N),qutip.qeye(2))
sigma = qutip.tensor(qutip.qeye(N),qutip.destroy(2))
sz = tensor(qeye(N),sigmaz())

#Defining Lindblad collapse operators

dephase = -np.sqrt(rate_phase)*sz
decay = np.sqrt(rate_1)*sigma
oscillator_loss = np.sqrt(kappa)*a

#Defining Jaynes_Cummings Hamiltonian

H = w*a.dag()*a-0.5*w0*sz + g*(a.dag()*sigma +a*sigma.dag())

#Defining qubit drive Hamiltonian
```

```
def Hd_coeff1(t, args):
    return np.exp(-1j*wd*t)


def Hd_coeff2(t, args):
    return np.exp(1j*wd*t)

Hd = [w*a.dag()*a-0.5*w0*sz, [l*sigma.dag(), Hd_coeff1],[l*sigma,Hd_coeff2]]
```

C.2 basic simulation

This section shows the code for performing a basic construction simulation.

```
field = (fock(N,5)+fock(N,2)).unit()
qubit = (basis(2,0)).unit()
init= tensor(field,qubit)
states,ts =simulate_construction(init,5,c_ops = [])
```

C.3 Decay and dephasing simulation

This section shows example code of how to simulate a construction using Lindblad collapse operators defined in C.1.

```
field = (fock(N,5)+fock(N,2)).unit()
qubit = (basis(2,0)).unit()
init= tensor(field,qubit)
states,ts =simulate_construction(init,5,c_ops = [decay,dephase,oscillator_loss])
```

C.4 Simple Wigner function

The code in this section shows how to generate a plot of a Wigner function of a state that is generated using the algorithm.

```
field = (fock(N,5)+fock(N,2)).unit()
qubit = (basis(2,0)).unit()
init= tensor(field,qubit)

states,ts =simulate_construction(init,5,c_ops = [decay,dephase,oscillator_loss])

xvec = np.linspace(-4, 4, 200)
final_state_wigner = wigner(states[-1].ptrace(0),xvec,xvec)
fig,ax = plt.subplots()

ax.contourf(xvec,xvec,final_state_wigner,100,norm=mpl.colors.Normalize(-0.25, 0.25),cmap=plt.get_cma
```

C.5 Plotting expectation value trace

```
field = (fock(N,5)+fock(N,2)).unit()
qubit = (basis(2,0)).unit()
init= tensor(field,qubit)
```

```
states,ts =simulate_construction(init,5,c_ops = [2*decay,dephase,2*oscillator_loss])

plt.plot(ts,expect(a.dag()*a,states))
```

C.6 Mesolve example

The following code shows an example of how to use the mesolve method with Lindblad collapse operators, Hamiltonian and options defined in C.1. The code also shows how to access the results of the mesolve method and use them to plot expectation values. In this case the qubit excitation probability is plotted.

```
field = (fock(N,5)+fock(N,2)).unit()
qubit = (basis(2,0)).unit()
init= tensor(field,qubit)

tlist = np.linspace(0, 200,401)
result = mesolve(H,init,tlist, c_ops = [decay,dephase,oscillator_loss],options = options

plt.plot(tlist,expect(sigma.dag()*sigma,result.states))
```